This manuscript is a preprint and has been submitted for consideration in **Tectonophysics**. It is our expectation that it will undergo peer review **after which it will hopefully be accepted for publication**. Subsequent versions of this manuscript may differ due to peer review or the editorial process. If accepted for publication, the final version will be available through the "Peer-reviewed publication DOI" link on this preprint server. We hope you find this paper interesting and would welcome your feedback on it.

Kindly contact Folarin Kolawole (folarin.kol@gmail.com or f.kolawole@columbia.edu) with any feedback that you may have.

Strain Localization and Migration During the Pulsed Lateral Propagation of the Shire Rift Zone, East Africa

Folarin Kolawole[1,2]*, Travis Vick[3,4], Estella A. Atekwana[5], Daniel A. Laó-Dávila[6], Aristides G. Costa[3], and Brett M. Carpenter[3]

[1]BP Exploration, Houston, TX 77079
[2]Lamont-Doherty Earth Observatory at Columbia University, Palisades, NY 10964
[3]School of Geosciences, University of Oklahoma, Norman OK 73019
[4]Department of Geophysics, Colorado School of Mines, Golden, CO 80401
[5]Department of Earth and Planetary Sciences, University of California, Davis, CA 95616
[6]Boone Pickens School of Geology, Oklahoma State University, Stillwater, OK 74078

**Corresponding Author: folarin.kol@gmail.com*

Key Points:

- Multiphase rifting in the Shire Rift Zone (SRZ) transitioned from earlier magma-rich phases (RP1 & 2) to the currently active magma-poor phase (RP3)
- Surface and subsurface data suggest a pulsed lateral SRZ propagation with transient rift-tip stagnation at/near rift-orthogonal basement shear zones
- Inherited intra-basement structures served as both strain-localizing and temporary strain-inhibiting tectonic elements during the rift propagation

Keywords: Continental extension, Multiphase rifting, Strain localization, Strain migration, Structural inheritance

Abstract

We investigate the spatiotemporal patterns of strain accommodation during multiphase rift evolution in the Shire Rift Zone (SRZ), East Africa. The NW-trending SRZ records a transition from magma-rich rifting phases (Permian-Early Jurassic: Rift-Phase 1 (RP1), and Late Jurassic-Cretaceous: Rift-Phase 2 (RP2)) to a magma-poor phase in the Cenozoic (ongoing: Rift-Phase 3 (RP3)). Our observations show that although the rift border faults largely mimic the pre-rift basement metamorphic fabrics, the rift termination zones occur near crustal-scale rift-orthogonal basement shear zones (Sanangoe (SSZ) and the Lurio shear zones) during RP1-RP2. In RP3, the RP1-RP2 sub-basins were largely abandoned, and the rift axes migrated northeastward (rift-orthogonally) into the RP1-RP2 basin margin, and northwestward (strike-parallel) ahead of the RP2 rift-tip. The northwestern RP3 rift-axis side-steps across the SSZ, with a rotation of border faults across the shear zone and terminates further northwest at another regional-scale shear zone. We suggest that over the multiple pulses of tectonic extension and strain migration in the SRZ, pre-rift basement fabrics acted as: 1) zones of mechanical strength contrast that localized the large rift faults, and 2) mechanical 'barriers' that refracted and possibly, temporarily halted the propagation of the rift zone. Further, the cooled RP1-RP2 mafic dikes facilitated later-phase deformation in the form of border fault hard-linking transverse faults that exploited mechanical anisotropies within the dike clusters and served as mechanically-strong zones that arrested some of the RP3 fault-tips. Overall, we argue that during pulsed rift propagation, inherited strength anisotropies can serve as both strain-localizing, refracting, and transient strain-inhibiting tectonic structures.

1 INTRODUCTION

The extensional deformation and break-up of the continental lithosphere often occur over multiple phases of stretching (Keep and McClay, 1997; Bergh et al., 2007; Mohriak and Leroy, 2013; Bell et al., 2014; Phillips et al., 2019a). Multiphase rifts may experience a rotation in extension direction between the different phases, leading to the geometrical modification of the earlier-established fault systems (Duffy et al., 2017; Bell et al., 2014; Henstra et al., 2015). Also, multiphase rifts commonly show evidence of complex patterns of spatial migration of strain and depocenters between the different phases, associated with the abandonment and later reactivation of the early rift faults, and/or creation of new fault systems (Ebinger et al., 2000; Bell et al., 2014; Brune et al., 2014; Ford et al., 2017; Fazlikhani et al., 2020). These processes facilitate the overall progressive growth of multiphase rift basins by the deepening, lengthening, and/or widening of the basin, demonstrated by an increase in the extent of the deformation.

As continental extension initiates, rift basins may attain significant width and length during the earliest phase of extension (e.g., Modisi et al., 2000; Rotevatn et al., 2018) and crustal strength properties may influence the lateral propagation of the rift tip (Van Wijk and Blackman, 2005). However, the recurrence of extension with prolonged inter-rift periods or decreased stretching rates could heal the mantle-lithosphere, and facilitate depocenter abandonment and migration of strain to an outboard zone of unrifted crust (e.g., Braun, 1992; Naliboff and Buiter, 2015). This outward migration of the crustal deformation leads to a progressive enlargement of the brittle deformation field, with associated crustal subsidence and rift-related sedimentary and/or volcaniclastic accumulation (Mohriak and Leroy, 2013; Naliboff and Buiter, 2015; Ford et al., 2017; Gawthorpe & Leeder, 2000).

Here, we examine the longstanding question of how evolving continental rifts propagate over multiple phases of tectonic extension, especially in the case of juvenile (stretching stage; low beta factor) rift settings. We explore this problem in the Shire Rift Zone (SRZ), East Africa (Figure 1a), which is one of the basins that experienced all the known phases of Phanerozoic extensional tectonics that affected the region. The NW-trending SRZ is located between the southern tip of the Malawi Rift, the Lower Zambezi Rift, and Urema Graben, and extends

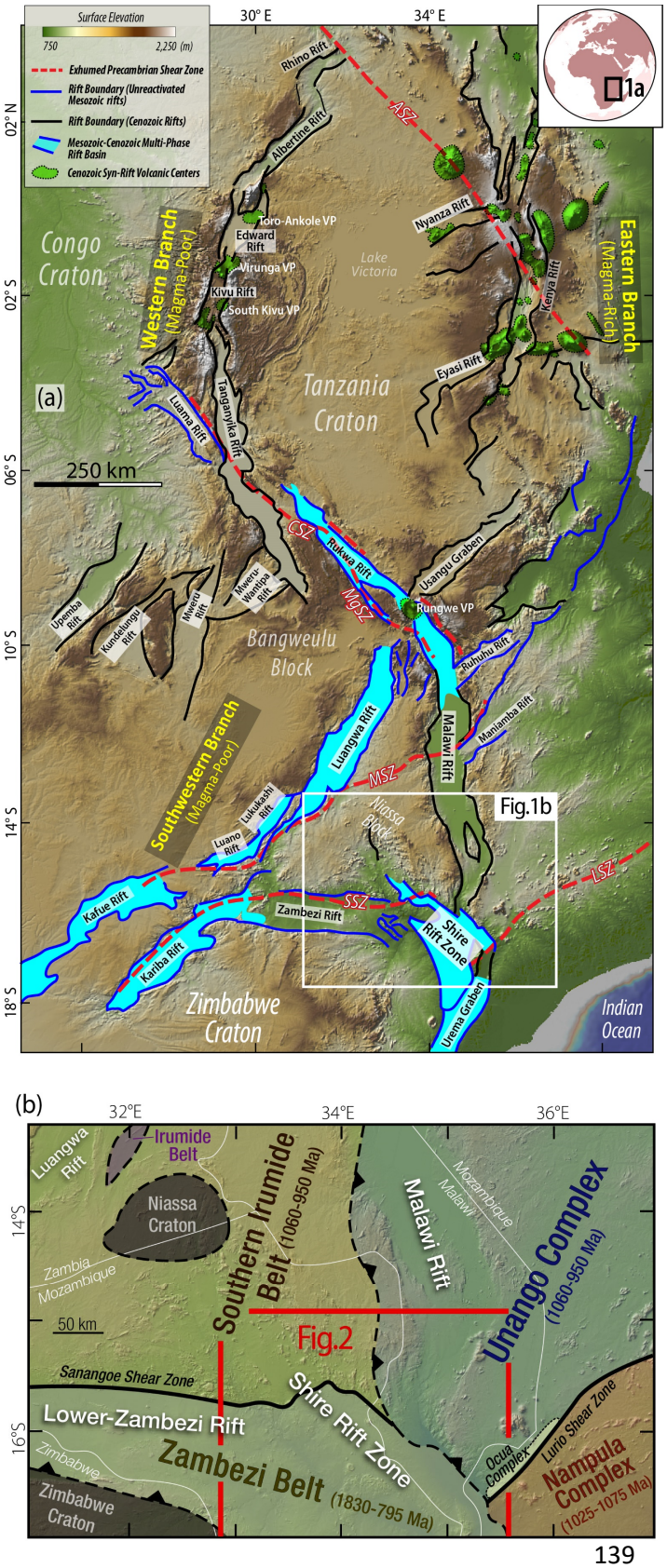

Figure 1. Regional tectonic setting. (a) Global Multi-resolution Topography (GMRT) digital elevation model (DEM) hillshade map of Eastern Africa showing the various segments of the East African Rift, and major Precambrian basement shear zones in the region (modified after Daly et al., 1989, Castaing, 1991; Delvaux, 1989; Fritz et al., 2013; Heilman et al., 2019). ASZ: Aswa Shear Zone, CSZ: Chisi Suture Zone, LSZ: Lurio Shear Zone, MgSZ: Mughese Shear Zone, MSZ: Mwembeshi Shear Zone, SSZ: Sanangoè Shear Zone. The blue polygons extend across rift segments with records of multiphase (Mesozoic-Cenozoic) extension and are not indicative of the part of the rift that was active during a particular phase of extension. GMRT source: Ryan et al. (2009). The GMRT base map is obtained from GeoMapApp. (b) Generalized map of the Precambrian basement terranes in the region of the Shire Rift (modified after Hargrove et al., 2003; Westerhof et al., 2008; Fritz et al., 2013). Although there is no clearly defined single shear zone separating some of the tectonic blocks (as indicated by dashed black lines), the Sanagngoe and Lurio shear zone terrane boundaries are well defined and constrained in field studies (Barr and Brown, 1987; Bingen et al., 2009). Sawtooth pattern on dashed lines indicates thrust relationship between the flanking terranes or basement blocks (after Westerhof et al., 2008).

139

140 across the political boundaries of Malawi and Mozambique (Figure 1b). The rift zone, which
141 developed within an exhumed Precambrian metamorphic crystalline basement (Figure 2),
142 exhibits excellent surface exposure of rift fault escarpments (Figure 3a), the pre-rift intra-
143 basement fabrics along the rift margins (Figures 3b-c), and multiphase syn-rift sedimentary
144 sequences within the rift basin and hanging walls of the rift-bounding faults (Figures 3a, 3d-
145 e).

146 We integrate field structural measurements, aeromagnetic data, digital elevation
147 model (DEM) hillshade maps, and published field and borehole data to investigate
148 multiphase rifting in the SRZ. Our study presents an updated structure of the rift zone,
149 highlighting the patterns of strain migration and how the rift transitioned from magma-rich
150 rifting into magma-poor rifting over three phases of tectonic extension. Also, the study
151 presents evidence suggesting that pre-rift crustal structures (and those inherited in earlier
152 rift phases) may influence rift evolution by playing the contrasting roles of 1.) weak,
153 exploitable structures that promote strain localization, and 2.) resisting structures that
154 transiently arrest or refract the lateral propagation of rift segments and associated faults.

155

156 ## 2 GEOLOGICAL SETTING

157 Eastern Africa has experienced multiple phases of extensional tectonic deformation
158 in the Phanerozoic Eon (e.g., Delvaux, 1989; Castaing, 1991; Chorowicz, 2005). These rifting
159 phases include the Permian – Early Jurassic (Karoo) rifting event herein referred to as rift-
160 phase 1 (RP1), a Late Jurassic - Cretaceous rifting event (rift-phase 2, RP2), and the current
161 Cenozoic phase of tectonic extension known as the 'East African Rift System' (rift-phase 3,
162 RP3). Some of the RP1 basins, among which is the SRZ, were reactivated during RP2, and
163 again reactivated in RP3 (Figure 1a; Delvaux, 1989; Castaing, 1991; Daly et al., 2020). The
164 SRZ is a NW-trending rift basin, flanked to the north by the N-trending Malawi Rift, to the
165 west by the E-trending Zambezi Rift, and to the south by the NNE-trending Urema Graben
166 (Figure 1a). Although the SRZ has been included as part of the Malawi Rift in some older
167 literature (e.g., Ebinger et al., 1987), following Castaing (1991), we distinguish the SRZ and
168 its sub-basins based on the distinct NW-SE trend of their border faults, onlapping syn-rift
169 sequences, and the basement-highs at the zones of interaction between the rifts (Kolawole

et al., 2021b). Each of the flanking rift segments, excluding the Urema Graben, are separated from the SRZ by a zone of exposed or shallowly-buried pre-rift basement, distinguishing the SRZ as a distinct tectonic element in the region (Castaing, 1991; Kolawole et al., 2021b).

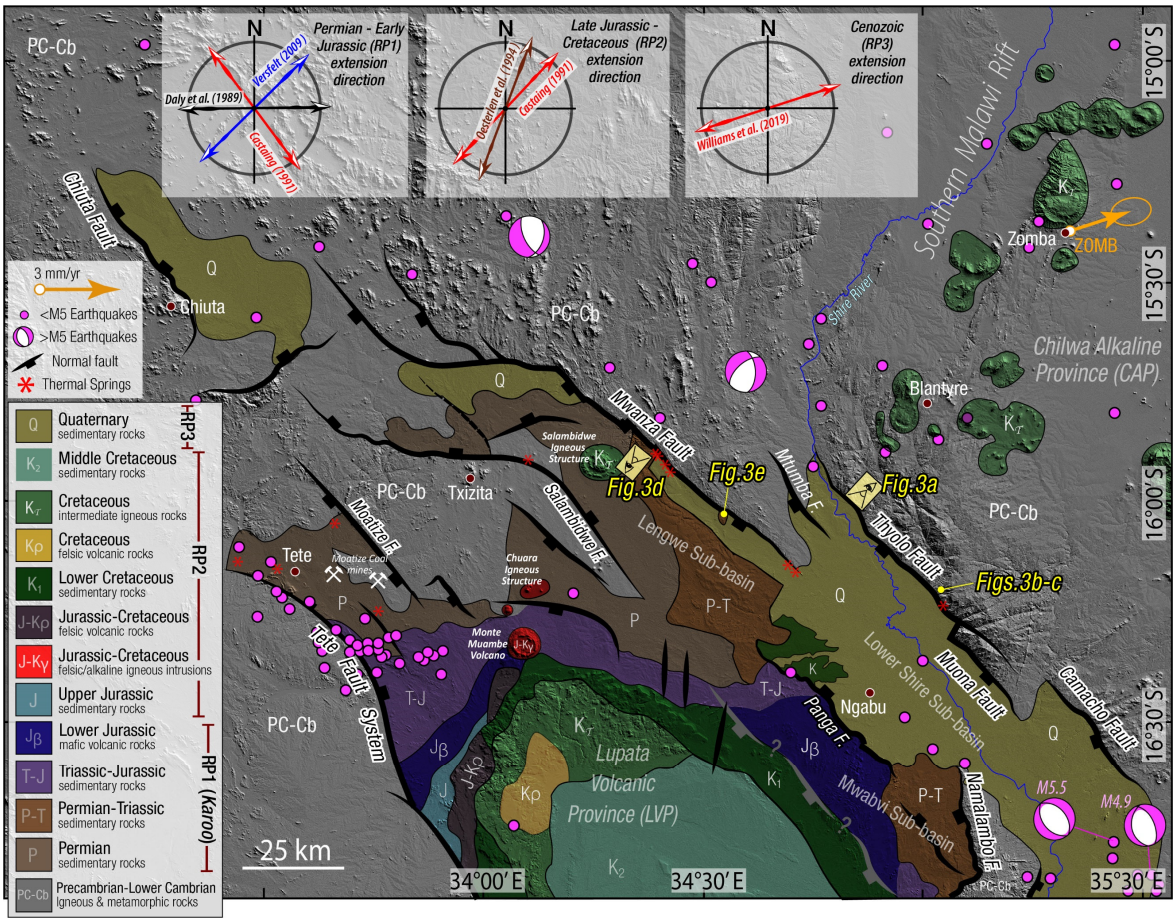

Figure 2. Geologic setting of the Shire Rift Zone. (a) Geologic Map of the Shire Rift Zone overlaid on Shuttle Radar Topography Mission (SRTM) digital elevation model. The map is compiled from Cooper and Bloomfield (1961), Habgood et al. (1963), Habgood (1973), Choubert et al., (1988), Bennett (1989), Castaing (1991), Chisenga et al. (2018), Nyalugwe et al. (2019a). *Top insets* show the inferred RP1 and RP2 regional extension directions from previous studies (Daly et al., 1989; Castaing, 1991; Oesterlen and Blenkinsop, 1994; Versfelt, 2009). The RP3 regional extension direction (Williams et al., 2019) was calculated from earthquake focal mechanism inversion. The orange arrow (ZOMB) represents the RP3 GNSS vector and velocity solution (with 95% uncertainty ellipse) for southern Malawi, from Stamps et al. (2018). Thermal springs are from Procesi et al. (2015), Njinju et al. (2019b), and Addison et al. (2021). Earthquakes are compiled from United States Geological Survey earthquake catalog, Williams et al. (2019), and Stevens et al. (2021). Note that seismicity in the Tete region is associated with coal mining operations in the Moatize coal mines Stevens et al. (2021).

2.1 The Pre-Rift Precambrian Basement

The SRZ extends along the tectonic boundaries separating four distinct Precambrian mobile belts and terranes (Figure 1b), which include the Southern Irumide Belt (1060 - 950 Ma), Zambezi Belt (1830 - 795 Ma), the Unango Complex (1060 - 950 Ma), and the Nampula Complex (1025-1075 Ma) (Hargrove et al 2003; Fritz et al., 2013). These mobile belts are composed of Paleoproterozoic-Mesoproterozoic crust which has been reworked and overprinted by contractional structures and igneous intrusions of the Neoproterozoic Pan African Orogeny. Overall, the mobile belts are dominated by schists, amphibolite and granulitic gneisses, and deformed granites, granodiorites, syenites, gabbro, and anorthosites (e.g., Figures 3b-c; Barr and Brown, 1987; Fritz et al., 2013).

Several field studies have revealed the presence of prominent crustal- and lithospheric-scale shear zones and sutures separating these basement terranes. These shear zones include the E- to ENE-trending Sanangoe Shear Zone (SSZ) separating the Southern Irumide Belt and Zambezi Belt (e.g., Barr and Brown, 1987; Kröner et al., 1997; Evans et al., 1999; Westerhof et al., 2008), and the NE-trending Lurio Shear Zone (LSZ) (Bingen et al., 2009; Sacchi et al., 2000; Westerhof et al., 2008) which defines the boundary between the Unango and Nampula Complexes (Figures 1a-b). The SSZ deformation is a 3 - 8 km wide zone of thrust duplexes and associated cataclasites (Barr and Brown, 1987), defining a crustal-scale south-dipping thrust boundary between two Proterozoic basement terranes: 1) the Tete Province to the south, within which the E- to ENE-trending gneisses, pelitic schists, and quartzites have been pervasively intruded by gabbroic plutons and anorthosites of the Tete Complex, and 2) the Luia Group Terrane to the north, which hosts gneisses, granulites and Charnockites (Barr and Brown, 1987; Evans et al., 1999). Based on the regional clustering patterns of deformed Proterozoic and Mesozoic alkaline rocks and carbonatites, it was inferred that the SRZ exploited a Late Proterozoic suture zone (Burke et al., 2003).

2.2 Multiphase Phanerozoic Rifting

The SRZ, which extends ~264 km along-strike and ~134 km in width (maximum width in the southeast), is defined by an area of fault-bounded syn-rift sedimentary and volcaniclastic sequences (Figure 2). The rift zone has undergone three distinct phases of

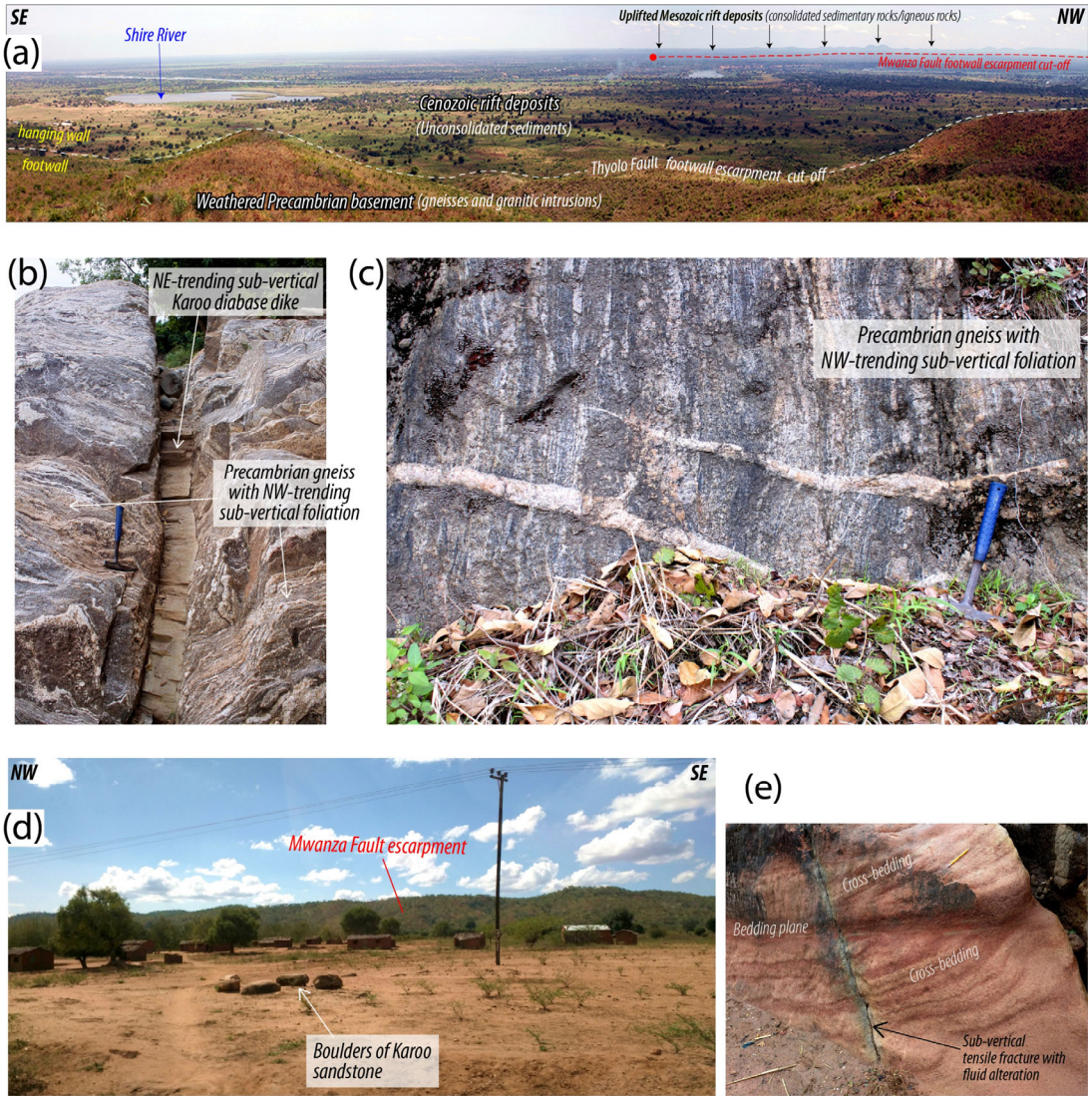

Figure 3. (a) Landscape photograph overlooking the Lower Shire River valley of the Shire Rift, looking southwest from the top of the Thyolo Fault escarpment (see location in Figure 2a). (b - c) Outcrops of Precambrian gneissic basement along the footwall of the Thyolo Fault showing NW-trending sub-vertical foliation. In Figure 3c, a sub-vertical NE-trending Jurassic diabase dike crosscuts the metamorphic foliation of the Precambrian gneiss host rock. (d) Landscape photograph looking northeast from the hanging wall of the Mwanza Fault. (e) Photograph of Karoo sandstone outcrop in the hanging wall of the Mwanza Fault. Also, see the locations of Figures 3b-e in Figure 2.

extension in post-Precambrian times (Figure 2; Castaing, 1991). The first episode of rifting (RP1), popularly known as the "Karoo" rifting episode, began in the Permian and ended in the Lower Jurassic (Castaing, 1991; Delvaux, 1989). This initial phase of extension established large >150 km-long basin-bounding master faults (border faults) which include

the SW-dipping Mwanza and Namalambo Faults to the northeast and a NE-dipping fault system (herein referred to as the 'Tete Fault System') to the southwest (Figure 2; Castaing, 1991). The early phase syn-rift fill is dominated by sedimentary sequences deposited in sub-basins defined by grabens and half grabens (Figures 2, 3d-e; Habgood, 1963; Choubert et al., 1988; Castaing, 1991). Among these RP1 sub-basins, only the Lengwe and Mwabvi domains have been studied in detail due to the widespread outcrops of the syn-rift units in Southern Malawi (Figure 2; Habgood, 1963; Castaing, 1991). RP1 was concluded by the emplacement of igneous centers and diabase dike swarms across the basin in the Early Jurassic, known as the Stormberg vulcanicity (e.g., diabase dike in Figure 3b; Habgood et al., 1963, 1973; Woolley et al., 1979). Studies of RP1 rifting in the region inferred contrasting orientations of regional extension direction (Figure 2 insets). Versfelt (2009) and Daly et al. (1989, 1991) proposed an E- to NE-extension direction, based on a broad kinematic interpretation of regional transtension driven by north-directed far-field compression from the south during the Gondwanide Orogeny (Daly et al., 1991; Trouw and De Wit, 1999). Whereas Castaing (1991) inferred a NW-extension direction, based on the presence of NE-trending Late RP1 Stormberg dike swarm in the Shire Rift Zone, assuming a dike-orthogonal dilatant opening direction (e.g., Fig. 3b).

The second phase of extension (RP2) was relatively short-lived, occurring between the Middle Jurassic and the Cretaceous (Castaing, 1991). RP2 extension was associated with the reactivation of the RP1 faults, voluminous expulsion of volcanic material and relatively minor clastic deposition and are well-documented in the southwestern (Lupata Volcanic Province, LVP), southeastern (Mwabvi sub-basin), and northeastern parts of the basin (Salambidwe Igneous Structure in the Lengwe sub-basin) (Castaing, 1991; Choubert et al., 1988). The magmatic activities also extended into areas outboard of the basin, particularly the Chilwa Alkaline Province (CAP; Figure 2; Cooper and Bloomfield, 1961; Nyalugwe et al., 2019a). The Cretaceous-age dikes are alkaline in composition with a set trending NE and another set trending NW (Castaing (1991). Although the stress inversion of slickenside striations obtained along major faults in the Lengwe and Mwabvi sub-basins show a 'post-Karoo' NE-SW mean extension direction, assuming a dike-orthogonal dilatant opening direction, Castaing (1991) proposed an initial minor NW-extension, but dominant NE-

298 extension direction for RP2. Based on strain analysis of slickenside striations and fault plane
299 orientations in Late RP1 and RP2 syn-rift units within the nearby Zambezi Rift (see Fig. 1a),
300 Oesterlen and Blenkinsop (1994) inferred an NNE-regional extension direction.

301 The third phase of extension (RP3) is associated with the currently active East African
302 Rift System. In the region of the SRZ, RP3 is thought to have begun in the Late Tertiary
303 (Delvaux, 1989) or Quaternary (Castaing, 1991), and is associated with localized deposition
304 of Quaternary sediments in the Lower Shire Valley of southern Malawi (Figures 2 and 3a;
305 Castaing, 1991; Chisenga et al., 2019) and the Chiuta area of Mozambique (Figure 2;
306 Choubert et al., 1988; Castaing, 1991). Although the RP1 and RP2 tectonic extension in the
307 SRZ were associated with widespread volcanism (magma-rich rifting), RP3 is non-magmatic.
308 The Quaternary Lower Shire depocenter (also known as "Shire Graben" or "Lower Shire
309 Graben") is bounded to the east by a system of SW-dipping normal faults which consist of
310 the Thyolo (Figure 3a), Muona, and Camacho Faults, and to the west by the Panga Fault
311 (Figure 2). The Panga Fault is interpreted to have initially developed within the hanging wall
312 of the Mwanza border fault during RP1 but had been reactivated in post-RP1 times marked
313 by the brecciation of a Late RP1 dolerite dike contained within the fault zone (Habgood,
314 1963; Castaing, 1991). In the Chiuta area, which is the northwesternmost sub-basin in the
315 SRZ, the west-bounding fault, herein referred to as "the Chiuta Fault", represents the border
316 fault in this part of the rift zone (Figure 2).

317 The SRZ exhibits a thinned lithosphere and elevated heat flow relative to the rift
318 flanks (Njinju et al., 2019a, 2019b). The RP3 regional extension direction is ENE- to E-W and
319 is responsible for several recent >Mw4 earthquakes in the basin (Figure 2; Williams et al.,
320 2019). Geodetic velocity solutions for the region show strain rates of ~2.2 mm/yr (Figure 2;
321 Stamps et al., 2018; Wedmore et al., 2021), and a geomechanical analysis shows that the RP3
322 eastern border faults are favorably oriented for reactivation in the regional stress field
323 (Williams et al., 2019). Although the broad geologic history of the SRZ has been identified in
324 previous studies (Habgood, 1963; Castaing, 1991), the major structural domains and
325 associated structural elements, the patterns of strain localization and migration, and
326 mechanics of rift propagation over its multiphase history remain unknown.

327

328 # 3 DATA AND METHODS

329 We integrated field observations from this study and previous studies, digital
330 elevation model (DEM) hillshade maps, intra-basinal borehole penetration logs, and
331 aeromagnetic data to generate an updated tectonic and structural framework for the SRZ,
332 allowing us to evaluate its multiphase rifting history.

333 To create an updated geologic map of the SRZ, we compile published geological maps
334 (Cooper and Bloomfield, 1961; Habgood, 1973; Habgood et al., 1963; Choubert et al., 1988),
335 which document field observations of the surficial geology across the rift basin and
336 surrounding areas. The compilation allows us to constrain the rift-related lithological units
337 and the spatial extents of the sub-aerial exposures and locations of juxtaposition against the
338 Precambrian basement. We integrated the published legacy geologic maps with subsurface
339 data from borehole penetrations (where available in the basin) and observations from
340 aeromagnetic fabric patterns beneath the rift basin deposits.

341 To provide an updated fault map of the rift zone, we first compiled fault lineaments
342 from the legacy geologic maps and previous studies in various parts of the rift (Choubert et
343 al., 1988; Castaing, 1991; Chisenga et al., 2018; Wedmore et al., 2020). These previous
344 studies mostly mapped faults from surface topographic scarps and outcrops but lack
345 information on the buried fault segments. Also, the mapping of potential buried faults from
346 linear gradients in a bouguer gravity grid covering the Malawi part of the basin (Chisenga et
347 al., 2018) is subject to the low resolution of the gravity data and lacks geological constraints.
348 To update the fault maps, we delineated additional fault segments using the vertical
349 derivative of the available aeromagnetic grids across the basin (Figures S1a-c). Although our
350 fault mapping mostly consists of buried faults and buried extensions of exposed faults
351 interpreted from filtered aeromagnetic maps, we also interpreted additional surface-
352 breaking fault segments from topographic hillshade maps (see Figure S2). Below, we provide
353 the details of the field data collection, borehole data, and aeromagnetic datasets, and data
354 analysis techniques used in the study.

355

356

357

3.1 Field Data

We conducted a field campaign in the Malawi part of the SRZ, covering the footwall and hangingwall areas of the Thyolo-Muona and Mwanza border fault systems (Figures 3a-e). In the exposures of the pre-rift gneissic basement along the footwalls of the rift border faults, we collected field measurements of the strike and dip of the metamorphic basement fabrics (i.e. foliation; n=39 along Mwanza Fault's footwall, and n=229 along Thyolo-Muona Fault's footwall). Along the footwall of the Thyolo-Muona Fault, where Mesozoic diabase dike intrusions are ubiquitous across the basement (e.g., Figure 3b), we collected field measurements of the strike and dip of the dikes where possible (n=50). We present the 3-dimensional (3D) structural datasets as equal-area stereographic projections of poles to planes with 2-interval Kamb contours. We augment our field measurements along the Thyolo-Muona Fault's footwall with datasets previously collected by the Geological Survey of Malawi and published in Habgood et al. (1973). The Geological Survey of Malawi structural dataset consists of strike/dip of gneissic foliation (n=191), and map-view traces of diabase dikes which we digitized and from which we automatically extracted 2,086 strike measurements of dike segments using ArcMap.

3.2 Shuttle Radar Topography Mission (SRTM) Digital Elevation Model (DEM)

In the less-studied sub-basins of the Shire Rift Zone, in combination with aeromagnetic data (see section 3.5), we utilized 1 arc-second (30 m spatial resolution) Shuttle Radar Topography Mission (SRTM) DEM hillshade maps to delineate surface traces of normal faults. In areas where the aeromagnetic data used in this study is of lower resolution (e.g., NW and SE termination zones of Shire Rift), we mapped the topographic lineaments in the DEM hillshade maps of basement exposures as supporting independent data on the trends of the basement metamorphic fabrics.

3.3 Aeromagnetic Data

For the mapping of buried fault segments, dikes, and buried volcanic centers, and the modeling of the depth-to-magnetic basement, we utilize two aeromagnetic datasets: a lower resolution (2 km spatial resolution) regional grid covering the entire basin (both the Malawi

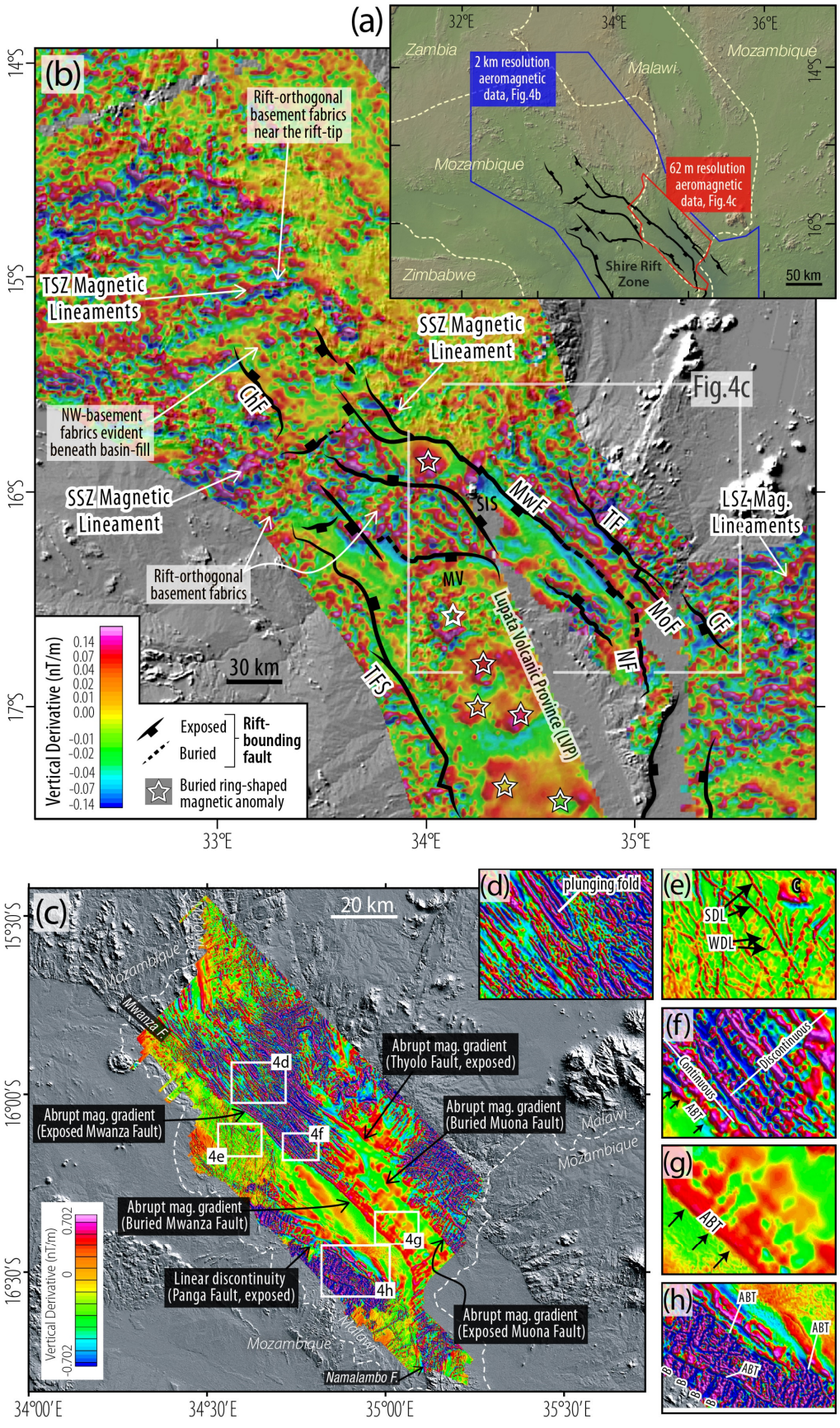
(a)
32°E
34°E
36°E
14°S
16°S
Zambia
Malawi
Mozambique
Zimbabwe
2 km resolution aeromagnetic data, Fig.4b
62 m resolution aeromagnetic data, Fig.4c
Shire Rift Zone
50 km
(b)
Rift-orthogonal basement fabrics near the rift-tip
TSZ Magnetic Lineaments
SSZ Magnetic Lineament
NW-basement fabrics evident beneath basin-fill
SSZ Magnetic Lineament
Rift-orthogonal basement fabrics
ChF
SIS
MwF
TF
MV
MoF
CF
NF
TFS
Lupata Volcanic Province (LVP)
LSZ Mag. Lineaments
Fig.4c
Vertical Derivative (nT/m)
0.14
0.07
0.04
0.02
0.01
0.00
-0.01
-0.02
-0.04
-0.07
-0.14
30 km
Exposed
Buried
Rift-bounding fault
Buried ring-shaped magnetic anomaly
15°S
16°S
17°S
33°E
34°E
35°E
(c)
20 km
15°30'S
16°00'S
16°30'S
34°00'E
34°30'E
35°00'E
35°30'E
Mozambique
Mwanza F.
Malawi
Abrupt mag. gradient (Thyolo Fault, exposed)
Abrupt mag. gradient (Exposed Mwanza Fault)
Abrupt mag. gradient (Buried Muona Fault)
Abrupt mag. gradient (Buried Mwanza Fault)
Linear discontinuity (Panga Fault, exposed)
Abrupt mag. gradient (Exposed Muona Fault)
Namalambo F.
4d
4e
4f
4g
4h
Vertical Derivative (nT/m)
0.702
0
-0.702
(d)
plunging fold
(e)
SDL
WDL
(f)
Continuous
Discontinuous
ABT
(g)
ABT
(h)
ABT
ABT
ABT

Figure 4. Aeromagnetic datasets. (a) Regional hillshade topography map (same as Fig. 1b) showing the coverage of the aeromagnetic datasets used in the study. (b) 1st vertical derivative of the regional-scale pole-reduced aeromagnetic grid (2 km spatial resolution) covering the Shire Rift and surrounding areas. CF: Camacho Fault, ChF: Chiuta Fault, LSZ: Lurio Shear Zones, MoF: Muona Fault, MV: Monte Muambe Volcano, MwF: Mwanza Fault, NF: Namalambo Fault, SIS: Salambidwe Igneous Structure, SSZ: Sanangoe Shear Zones, TSZ: Techigoma Shear Zone. The delineation of the shear zones (LSZ and SSZ) is constrained by field observations in Barr and Brown (1987); Sacchi et al. (2000), Kroner et al. (1997), Bingen et al. (2009), Fritz et al. (2013). (c) 1st vertical derivative of the higher-resolution pole-reduced aeromagnetic grid (62 m spatial resolution) covering only the Malawi part of the rift basin. Salient aeromagnetic fabric patterns observable in the high-resolution aeromagnetic map include: (d) Broad clusters of parallel, elongate magnetic fabrics in the exposed basement (i.e. basement metamorphic foliation). (e) Cross-cutting discrete magnetic-high lineaments enclosed by magnetic-low anomalies (i.e. mafic igneous dikes in sedimentary strata). 'SDL': Strong discrete lineament (shallow dike), 'WDL': Weak discrete lineament (deep-seated dike), 'C': Discrete magnetic-high ring-shaped anomaly (ring intrusion or sill?). (f) Mesh pattern fabrics in the exposed basement (i.e. metamorphic foliation overprinted by cross-cutting mafic dikes). (g) Mesh pattern fabrics in the buried basement (i.e. buried part of the basement exposed in Figure 3f). (h) Compact linear bands of chaotic magnetic fabrics (i.e. exposed or shallowly buried mafic volcanic deposits). The fabric becomes diffused northeastward as the depth of burial of the volcanic flows increases. 'B': compact band, 'ABT': abrupt magnetic gradient (i.e. normal fault). See Figures S1a-c for unfiltered and uninterpreted versions of the aeromagnetic grids. The unfiltered total magnetic intensity grids of these vertical derivative maps are in supplementary figures S1a-c.

and Mozambique sections) and surrounding areas (Figures S1a-b, 4a-b), and a higher resolution (62 m spatial resolution) grid covering only the Malawi section of the basin (Figures S1c, 4a, and 4c). The regional dataset (Figure S1a) consists of a grid of merged aeromagnetic field data acquired in the 1970s and 1980s from countries in southern Africa (source: South Africa Development Community, SADC aeromagnetic data, provided by Council for Geoscience, South Africa). This regional data includes a legacy Malawi aeromagnetic grid which has a resolution of ~250 m spatial resolution and was acquired in 1984/1985 with a 120 m terrane clearance and 1 km-spaced NE-SW flight lines (Figure S1b; Kolawole et al., 2018). The 62 m-resolution Malawi aeromagnetic data (Figure S1c) was acquired in 2013 (source: Geological Survey Department of Malawi; Nyalugwe et al., 2019b) with 80 m terrane clearance along NE-SW lines with a line spacing of 250 m.

3.4 Borehole Data

To investigate the subsurface stratigraphy in the RP3 Lower Shire Sub-basin, we assessed available lithologic logs from borehole penetrations below the Quaternary sediments, which are documented in Habgood (1963) and Habgood et al. (1973) (Figure S3a-b). There is no known documentation of well penetration beneath the Quaternary sediments

in the RP3 Chiuta Sub-basin. Therefore, to infer the dominant basin fill of the Chiuta Sub-basin, we relied on published surficial geologic maps, aeromagnetic fabric analysis, and lateral variations in DEM hillshade surface roughness patterns across the sub-basin.

3.5 Structural Interpretation from Aeromagnetic Data

Although structural deformation is commonly expressed as 'abrupt' gradients in aeromagnetic grids, the distinct magnetic character and expressions of basement-rooted fault traces, cross-cutting mafic dike intrusions, dike-intruded fault zones, and exhumed metamorphic terrane fabrics can be distinguished (Jones-Cecil et al., 1995; Modisi et al., 2000; Kinabo et al., 2007, 2008; Grauch & Hudson, 2007; Kolawole et al., 2018; 2017; Heilman et al., 2019). The total magnetic intensity (TMI) aeromagnetic data is a grid of magnetic anomalies produced by a combination of the magnetic susceptibility of the sources, the depth to the top of the magnetic sources, and the steepness of the contacts between distinct magnetic bodies [e.g., Grauch & Hudson, 2007, 2011]. However, due to the vertical offset and lateral juxtaposition of layers of strongly contrasting magnetic properties across steep fault planes, derivative-filtered aeromagnetic grids can resolve both buried and surface-breaking normal faults that offset the primary magnetic units. Similarly, the lateral alternation of mafic and felsic mineral banding in gneissic rocks (metamorphic basement fabrics), and mafic dikes cross-cutting gneissic basement are resolvable by derivative aeromagnetic grids which allows the delineation of their large-scale trends (Kinabo et al., 2007, 2008; Kolawole et al., 2018; Heilman et al., 2019; Lemna et al., 2019). Thus, the aeromagnetic datasets covering the SRZ allow us to delineate the rift-related faults (sub-aerial and subsurface), buried and sub-aerial magmatic structures (dikes and ring-shaped intrusions), and pre-rift basement fabrics within the Shire Rift and along its margins.

However, before structural interpretation, we first pole-reduced (RTP) the total magnetic intensity (TMI) aeromagnetic datasets to correct for the skewness of the magnetic field due to the proximity of the study area to the equator (Baranov, 1957; Arkani-Hamed, 1988). Here, we preferred RTP correction over equator-reduction (RTE) because the RTP correction produced a grid with better alignment of fault-related gradients with their geologic sources in areas where the surface breaking fault traces provide geologic

484 constraints (see Kolawole et al., 2018). After RTP correction, we applied a vertical derivative
485 filter to the TMI-RTP data to better resolve the structure-related gradients in the grids
486 (Figures 4b-h) (e.g., Ma et al., 2012; Kolawole et al., 2017; 2018; Heilman et al., 2019).
487 Following a systematic characterization of the aeromagnetic patterns observable in the 2013
488 Malawi aeromagnetic grid (Figures 4d-4h), we identified distinct patterns herein referred to
489 as 'aeromagnetic facies', which allow a better interpretation of the structural character of the
490 associated magnetic sources. To assess the orientation of basement foliation and mafic dikes
491 in the SRZ, independent of the collected field measurements (see section 3.1), we digitized
492 and measured the trend of the aeromagnetic anomaly lineaments corresponding to the
493 structures constrained by published geologic map of the basement structures (Habgood et
494 al., 1973). In the Mozambique part of the SRZ where a lower-resolution aeromagnetic data
495 is available (Figure S1), we supplemented aeromagnetic mapping with the digitization and
496 trend measurement of topographic lineaments representing basement fabrics.

497 Further, we calculated the frequency-azimuth distribution of the measured lineament
498 trends within the relevant segments of the rift zone. For multimodal distributions, we
499 divided the data into their modal sets using the frequency minima. For both unimodal and
500 multimodal plots, we calculated the circular vector mean and 95 % confidence interval for
501 the modal sets using the method of Mardia and Jupp (2009). Note that the magnitude of the
502 confidence interval is dependent on the number of sample data used. All frequency-azimuth
503 plots present in this study are area-weighted.

504

505 **3.6 Estimation of Depth-to-Magnetic Basement**

506 Along the SRZ, we estimated the depth-to-magnetic basement in two sub-basins
507 where a widespread accumulation of Quaternary-age sediments is most widespread and
508 prominent. These sub-basins are in the Chiuta Fault hanging wall and the Lower Shire
509 Graben (Thyolo-Muona Fault hanging wall) with extensions into the Mwanza Fault hanging
510 wall (Figure 2). In the Chiuta area, which is in Mozambique, we utilized the available 2 km-
511 resolution regional aeromagnetic grid (Figures S1a and 4b). Whereas, in the Lower Shire
512 Graben, located in Malawi, we utilized the original (unmerged) Malawi part of the legacy
513 regional grid (Figure S1b). Our preference for the unmerged legacy Malawi aeromagnetic

514 grid for source-depth estimation is due to its moderate resolution and suppression of high-
515 frequency noise (e.g., related to intra-sedimentary mafic dikes).

516 To perform an automatic calculation of depth-to-the top of the magnetic basement,
517 we used the Source Parameter Imaging™ (SPI™) transform of the aeromagnetic grid
518 (Thurston and Smith, 1997; Smith et al., 1998). The SPITM technique assumes a step-type
519 source model and produces spatially distributed source depth-solutions that are
520 independent of magnetic declination, inclination, strike, dip, and remanent magnetization.
521 The transform first computes the tilt derivative, and the total horizontal gradient of the tilt
522 derivative (local wavenumber, K). For a step source model, the Kmax-1 represents the depth
523 to the magnetic source where Kmax is the peak value of the local wavenumber based on a
524 simple Blakely test (Blakely and Simpson, 1986). Following standard practice, to minimize
525 the noise from shallow sources, we applied a Hanning filter to the K grid before calculating
526 the source depths. The gridding of the depth solutions assumes a 2-layer model such the SPI
527 map represents the average depth to the top of the shallowest magnetic basement. Source
528 depth estimations from aeromagnetic data generally have an accuracy of about ±20 % (Gay,
529 2009), thus, they provide a coarse approximation of lateral variation of depth to the top of
530 the magnetic basement beneath the rift sedimentary deposits.

531

532 # 4 RESULTS

533 ## 4.1 Structural Compartmentalization of the Shire Rift Zone (SRZ)

534 The updated fault map of the SRZ (Figure S2), integrated with the existing geologic
535 map of the basin (Figure 2), provides information on the structure and sub-basinal
536 compartmentalization of the rift zone. The large-scale rift architecture is defined by a NW-
537 trending basin that bifurcates northwestwards into two 20-25 km-wide grabens, both of
538 which are bound by large fault systems (Figure 5a). Based on the distribution and ages of
539 rift-related sedimentary and volcaniclastic units within the confines of these faults (Figure
540 2), we identify seven sub-basins (Figure 5b). These sub-basins include five magmatic sub-
541 basins: Lengwe, Mwabvi, Moatize, Monte-Muambe, and Lupata, which host RP1 and RP2
542 volcano-sedimentary sequences; and two non-magmatic sub-basins: Lower Shire and Chiuta
543 where widespread RP3 Quaternary sedimentary cover is localized (Figures 2 and 5b). The

Lupata Sub-basin hosts a major Mesozoic volcanic zone, the Lupata Volcanic Province (LVP). The LVP and the Salambidwe Igneous structure define the main intra-rift igneous zones, and the Chilwa Alkaline Province (CAP) defines an off-rift syn-rift igneous province.

Basin-scale rift-orthogonal topographic profiles (profiles P1 to P3; Figures 5a-b) show that the most-prominent topographic-highs in the SRZ are the southwestern and northeastern flanks of the Chiuta Sub-basin, the Salambidwe Igneous Structure, the eastern flank of the Lengwe Sub-basin, and the eastern flank of the Lower Shire Sub-basin. However, the escarpment height of the border fault zones (Figures 5c-e) is largest in the southwestern margin of the Chiuta Sub-basin (~696 m) and in the northeastern margin of the Lower Shire Sub-basin (~708 m), and smallest in the northern margins of the Lengwe Sub-basin (<200 m) and the southwestern margin of the Lupata Sub-basin (66 m). Along the entire rift, the border faults with the greatest escarpment height are the Chiuta Fault and the Thyolo-Muona Fault system.

At the northwestern tip of the SRZ (Chiuta Sub-basin), the rift morphology defines a graben geometry in which the basin asymmetrically tilts gently westwards towards the Chiuta border fault (profile P1, Figure 5c). At the central part of the rift zone (profile P2, Figure 5b), the rift morphology highlights the western and eastern rift bifurcations (Moatize and Lengwe Sub-basins), separated by a basement block, which we herein refer to as 'the Txizita Horst' (after 'Txizita town' in Figure 2). In the southeast, the SRZ is widest, defined by a ~134 km-wide basin in which the western and central areas (Lupata and Mwabvi Sub-basins) are elevated relative to the far eastern areas (Lower Shire Sub-basin) (profile P3, Figure 5c). Although the Quaternary sediments of the Lower Shire Sub-Basin onlap the Mesozoic sequences in the Lengwe and Mwabvi Sub-basins, a major boundary between the Mwabvi and Lower Shire is marked by the NE-dipping Panga Fault such that the Mwabvi is in the SW and Lower Shire in the NE. The surface morphology of the Lower Shire Sub-basin reflects a graben morphology in which the basin asymmetrically tilts eastwards towards the Thyolo-Muona-Camacho border fault system. However, all the aeromagnetic grids over the Lower Shire Graben (e.g., Figures S1a-c) and depth-to-basement map (see section 4.2.1) show that this sub-basin is further compartmentalized into a deeper SW section and shallower NE section by the buried southeastern continuation of the Mwanza Fault

4.2 Subsurface Structure of the Active Sub-Basins in the Shire Rift Zone

In the SRZ, the sub-basins that host widespread accumulations of Quaternary sediments are inferred to be active in the current phase of rifting in eastern Africa. Although the most prominent of these sub-basins are the Lower Shire and Chiuta Sub-basins (Figure 2), we also note that the northern and southern Lengwe Sub-basin show evidence of partial reactivation (see partial Quaternary sediment cover in Figure 2). An understanding of the first-order subsurface structure of the two prominent RP3 sub-basins is critical for elucidating the multiphase evolution of the SRZ.

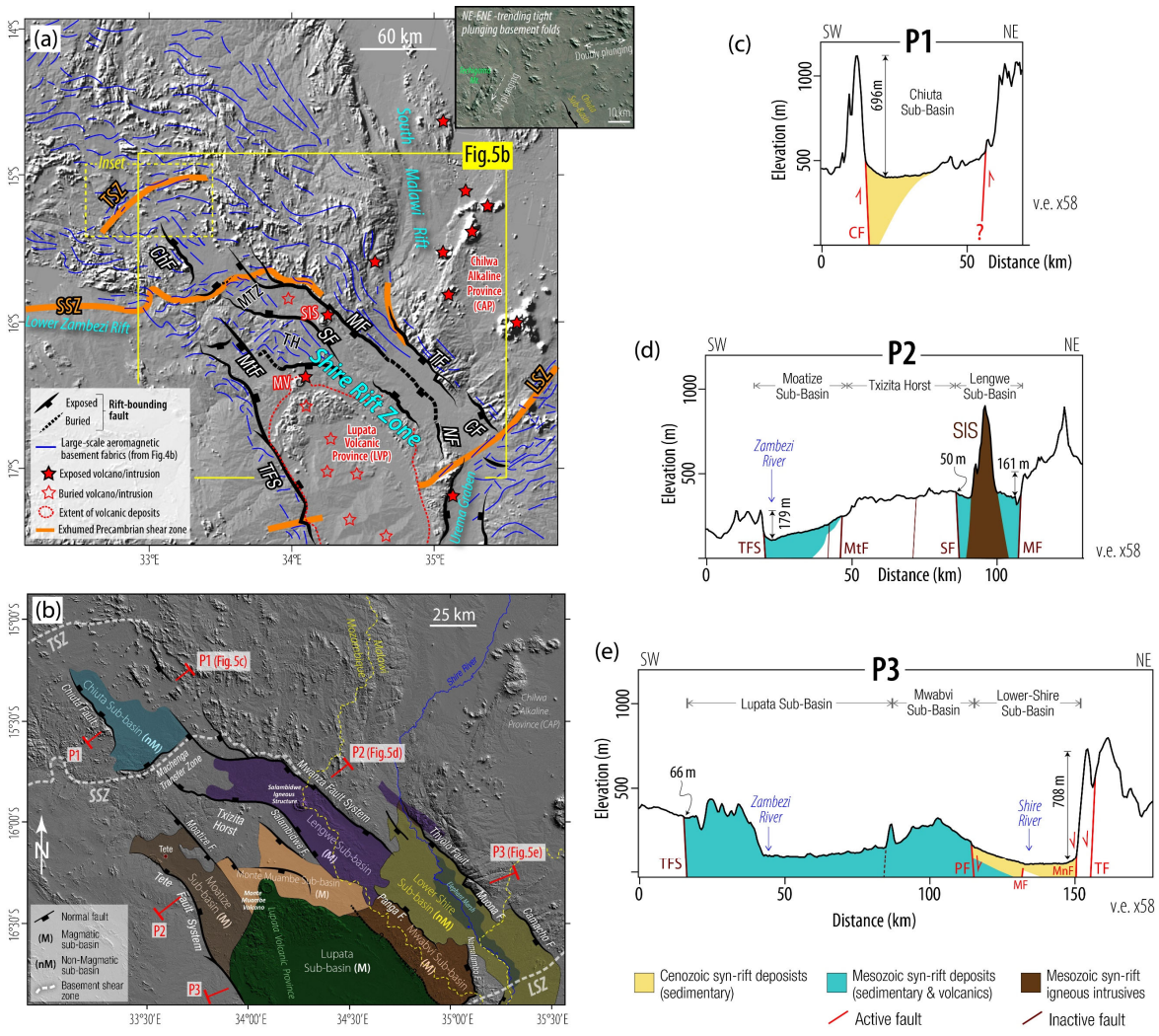

Figure 5. New Interpretation of the Large-Scale Structure of the Shire Rift Zone. (a) Hillshade digital elevation model overlaid with interpretations of the filtered regional aeromagnetic data. Open and filled red stars are Mesozoic (RP1-RP2) igneous centers. CF: Camacho Fault, ChF: Chiuta Fault, LSZ: Lurio Shear Zone,

603 MDC: Mulata Dike Cluster, MF: Mwanza Fault, MtF: Moatize Fault, MV: Monte Muambe Volcano, NF: Namalambo
604 Fault, SF: Salambidwe Fault, SIS: Salambidwe Igneous Structure, TF: Thyolo Fault, TFS: Tete Fault System, TH:
605 Txizita Horst, TSZ: Techigoma Shear Zone. The location, geometry, and extents of the Lurio and Sanangoe Shear
606 Zones are after Barr and Brown (1987); Sacchi et al. (2000), Kroner et al. (1997), Bingen et al. (2009), Fritz et
607 al. (2013). The Techigoma Shear Zone is delineated in this current study based on its character as a distinct
608 high-amplitude aeromagnetic lineament separating terranes of different fabric trends (Figure 2b), collocated
609 with satellite-scale, plunging tight folds (inset showing Google Earth map). (b) Map showing the Shire Rift
610 extents and sub-basin compartmentalization based on fault scarp continuity and published distribution of the
611 syn-rift sedimentary and volcanic deposits (Figure 2; Choubert et al., 1988). LM: Lake Mbenje, LSV: Lurio Shear
612 Zone, SSZ: Sanangoe Shear Zone. (c - e) Rift-perpendicular topographic profiles (see Figure 5b for profile
613 transects).
614

615 *4.2.1 Depth to Magnetic Basement*

616 *The Lower Shire Sub-Basin:*

617 The spatial distribution of depth-to-magnetic basement estimates beneath the Lower
618 Shire (Figure 6a) shows larger depths in the hanging walls of the Mwanza-Namalambo Fault
619 System compared to the hanging walls of the Thyolo-Muona Fault System. The results show
620 that along the Mwanza Fault's hanging wall, the magnetic basement depths range between
621 ~900 m and 2.4 km and attain a maximum of ~2.7 km at locations within both the exposed
622 and buried sections of the fault. The hanging wall of the Namalambo Fault exhibits shallower
623 depths than that of the Mwanza Fault but attains a maximum depth of 2.4 km along its
624 southern section. Whereas, relative to the Mwanza-Namalambo Fault, the magnetic
625 basement in the hanging wall of the Thyolo-Muona Fault defines a broad 'shelf' area with
626 depths mostly ranging between 600 m and 1.2 km but records a maximum of ~1.4 km near
627 the central areas of the hanging wall.

628 Overall, the hanging wall of the Mwanza Fault features broader and deeper zones of
629 basement-lows compared to the Thyolo-Muona Fault hanging wall which shows smaller
630 zones of basement-lows with moderate depths, separated by NW and NE-trending
631 basement-highs. Thus, although the hanging walls of Mwanza and Thyolo-Muona synthetic
632 border fault systems are covered by widespread Quaternary syn-rift sedimentary deposits
633 (Figures 2 and 5e), the subsurface basement structure reveals significant contrast in the
634 magnitudes of subsidence of the magnetic basement across the border faults.

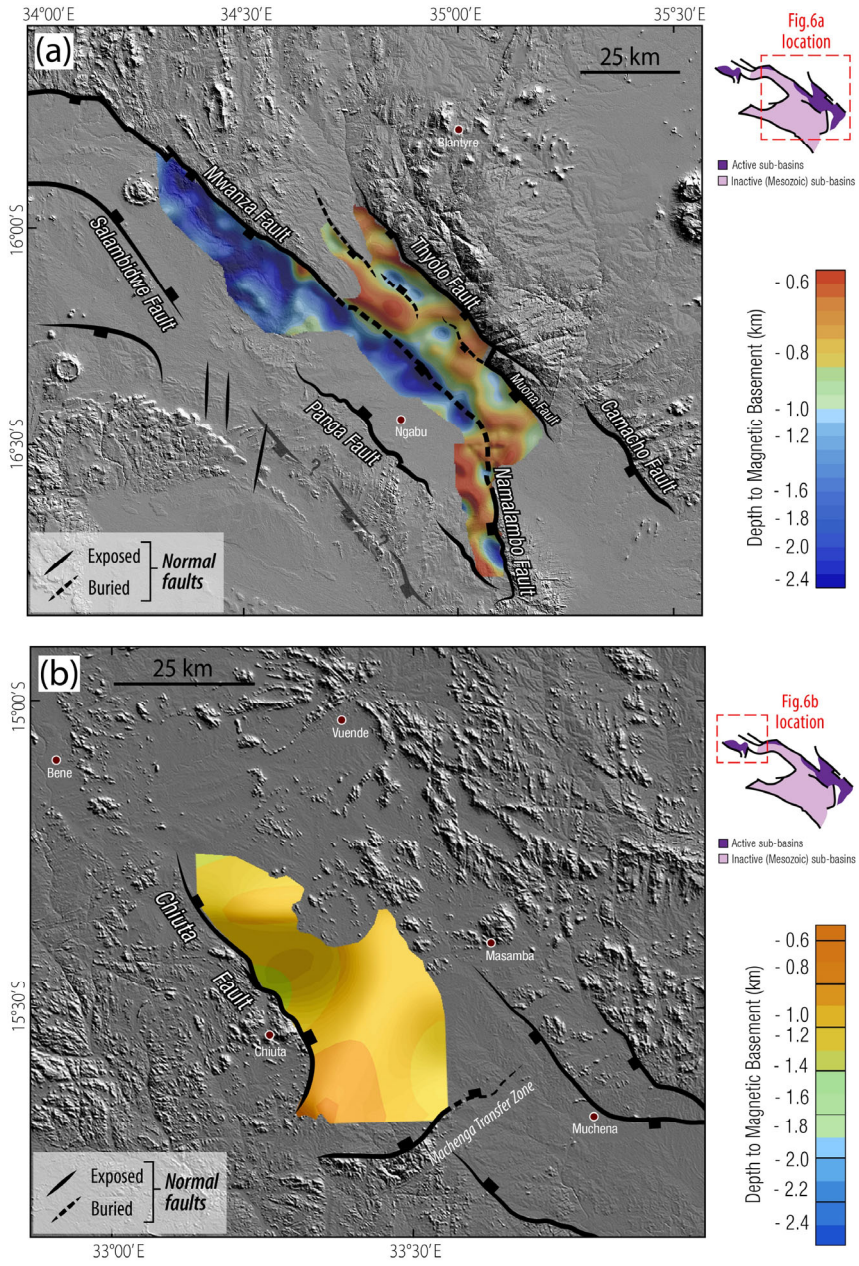

Figure 6. Depth-to-Magnetic Basement in the active (i.e., Cenozoic) Sub-Basins. (a) Depth-to-magnetic basement map of the Lower Shire sub-basin (and part of the Lengwe Sub-basin), overlaid on Shuttle Radar Topography Mission (SRTM) digital elevation model (DEM) hillshade map. The top of RP2 volcanic sequences is inferred to represent the magnetic basement in the hanging wall of the Mwanza-Namalambo Fault (Domains 1 & 2 in Fig. 7c). Whereas the top of the pre-rift metamorphic basement most likely represents the magnetic basement to the northeast of the Mwanza Fault (Domains 3-4 in Fig. 7c). (b) Depth-to-magnetic basement map of the Chiuta sub-basin, overlaid on SRTM-DEM hillshade map. Here, due to a lack of evidence on the presence of Mesozoic volcanics in this sub-basin, the top of the pre-rift metamorphic basement is inferred to represent the magnetic basement. Note that the Lower Shire sub-basin depth map shows a higher resolution than that of the Chiuta sub-basin because of the relatively higher-resolution aeromagnetic data in the Lower Shire sub-basin (see Figs. 3b-c).

The Chiuta Sub-Basin:

The results (Figure 6b) show that the magnetic basement generally deepens southwestwards towards the Chiuta Fault, attaining a maximum depth of ~1.4 km. To the southeast, the basement first shallows up to ~1 km before deepening slightly to ~1.2 km along a NE-trending, NW-dipping fault that terminates the sub-basin against the 'Machenga Transfer Zone'. Due to the absence of borehole penetration data in the Chiuta sub-basin, the lateral variation in our depth-to-magnetic basement estimate provides the first insight into the subsurface structure of the sub-basin.

4.2.2 Basement and Stratigraphic Architecture of the Lower Shire Sub-Basin

The Quaternary deposits in the Lower Shire Sub-basin overlap with the Mesozoic syn-rift deposits of the Lengwe and Mwabvi Sub-basins (Figure 2). Thus, with illustrations in Figures 7a and 7b, we describe here our observations of the basement and syn-rift architecture of the Lower Shire Sub-basin relative to those of its bounding sub-basins.

The Mwabvi Sub-basin is dominated by RP1 volcano-sedimentary units with no known accumulation of Quaternary (RP3) sediments (Domain-1 in Figure 7a). The Lengwe Sub-basin is also dominated by the RP1 units but hosts minor accumulations of RP3 sediments (Figure 2) in the northern segments of the Mwanza Fault (Domain-2 in Figure 7b). Along the northern Mwanza Fault, the syn-rift sequences are directly juxtaposed against the Precambrian metamorphic basement exposed in the footwall of the fault (Domain-3 in Figure 7b). However, towards the southeast, the cover of RP3 sediments in Domain-2 is more widespread and dominates the surficial extents of the domain.

Integration of all available information from independent datasets provides insight into the syn-rift stratigraphic architecture and lateral variation in the origin of the magnetic basement across the Lower Shire Sub-basin. These datasets include field observations (Figures 3a-c), basin-scale surficial geological map compilation (Figure 2), litho-logs from boreholes that penetrate below the Quaternary sedimentary cover (S3a-b and Table S1), and aeromagnetic fabric patterns (Figures 4c-h). First, these datasets show that the RP1-RP2 volcano-sedimentary units of the Mwabvi Sub-basin have been faulted and buried beneath RP3 sediments on the hanging wall of the Panga Fault (Domain-1 and -2 in Figure 7c).

Second, borehole logs and the aeromagnetic fabric patterns show that the RP1-RP2 volcanic rocks do not extend into the footwall of the buried Mwanza Fault segments (Figures 7c, S3a-b; Table S1). Also, the logs from boreholes in the areas between the Mwanza Fault and Thyolo Fault show no evidence for the presence of RP1 or RP2 sedimentary rocks beneath Quaternary sediments as the unconsolidated sediments directly overlie the gneissic basement (Figure S3a; Table S1). The magnetic structure of the Lengwe Sub-basin where mafic dikes have intruded the Mesozoic sedimentary sequences (Figure 7b) is different from that of the hanging wall of the Thyolo-Muona Fault system where high-amplitude anomalies are sparse and are of long-wavelengths. This suggests that there is no magnetic fabric pattern defining mafic diking of the sedimentary sequences overlying the gneissic basement in the hangingwall of the Thyolo Fault (Domain-3 in Figure 7c).

Additionally, beneath the Cenozoic cover of the Thyolo-Muona Fault hanging wall, the aeromagnetic map reveals a long-wavelength, low-frequency gradient that is parallel to- and extends northeastwards from the NE surface termination of the Muona Fault (Figure 4c). We describe this gradient as representing a buried (non-surface-breaking) segment of the Muona Fault. Based on these observations, we present an updated and comprehensive structural map of the Shire Rift, showing the previously mapped features and those mapped in this study (Figure 8).

4.2.3 Basement and Stratigraphic Architecture of the Chiuta Sub-Basin

The absence of high-resolution aeromagnetic data over the Chiuta Sub-basin does not permit a detailed structural interpretation. However, a key observation here is that aeromagnetic lineaments corresponding to a continuation of basement metamorphic fabrics beneath the rift-fill are visible along the axis of the Chiuta Sub-basin (Figure 4b). This is consistent with observations in other juvenile rift basins in Eastern Africa where the shallowly buried metamorphic basement is directly overlain by non-magnetic unconsolidated sediments (Kinabo et al., 2007; Kolawole et al., 2018),

4.3 Pre-Rift Basement Metamorphic Fabrics of the Shire Rift Zone (SRZ)

In the areas of exposed basement along the SRZ, aeromagnetic facies representing the basement metamorphic fabrics (gneissic foliation) are defined by tight clusters of parallel, elongate magnetic lineaments that show folded geometries along their strike (e.g., Figure 4d). We herein refer to this aeromagnetic pattern as the 'basement metamorphic fabric' or 'basement fabric'. Also, during our field visit, where possible, we collected strike and dip measurements of the basement foliation to independently compare with the broader-scale measurements from aeromagnetic grids. Below, we summarize the results of the frequency-azimuth distribution of the mapped basement fabrics observed along the SRZ (Figures 9a-g).

4.3.1 The Mwanza and Thyolo-Muona Border Faults and Environs

Along the Mwanza Fault, the frequency-azimuth distribution of the basement fabric (Figure 9bi) shows a dominant NW-SE trend with a 140° mean trend that is sub-parallel to the fault trend (~136°). This is consistent with our field measurements of the basement foliation (stereographic projection inset in Figure 9bi). Along the Thyolo-Muona Fault system, the mapped aeromagnetic metamorphic fabrics also show a prominent NW-SE trend with a mean of 123° (Figure 9ci), which is consistent with field measurements (128°), both being parallel or sub-parallel to the fault trend (~131°). We also note that along both the Mwanza and Thyolo Faults, the average dip magnitude and dip direction of the basement fabrics are strongly correlated with those of the faults (see stereographic contours and poles to fault planes in Figures 9bi and 9ciii).

4.3.2 Txizita Horst

In the absence of high-resolution aeromagnetic data over the Txizita Horst, we map basement fabrics in both the low-resolution SADC aeromagnetic grid (Figures 4b, 5a) and the topographic relief map (red lines in Figure 9a). The frequency-azimuth distributions of the metamorphic fabric lineaments in both datasets (Figure 9di-ii) show a multimodal distribution with consistent dominant sets trending ENE to NE (~079° from aeromagnetics, ~069° from topographic relief) and NW-SE (~132° from aeromagnetics, 145° from topographic relief). The plots also show a minor N to NNE set (~011° from aeromagnetics,

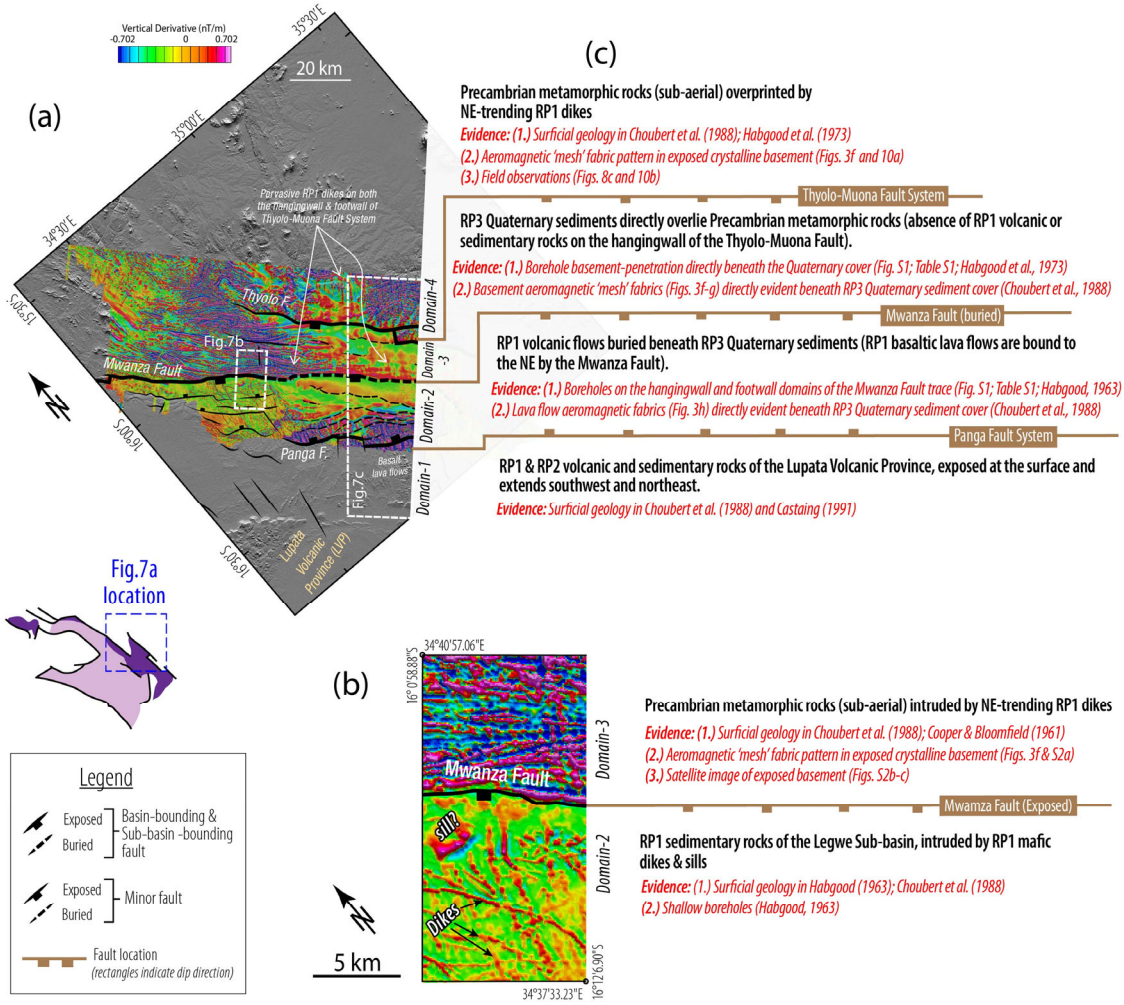

Figure 7. Borehole and magnetic fabric constraints on the relative timing of strain localization in the Lower Shire sub-basin. (a) Map covering parts of the Lengwe and Lower Shire sub-basins (same map in Figure 3c). (b) Zoomed-in map of the eastern portion of the Lengwe Sub-basin (see location in inset sketch map). The interpretations of the distinct magnetic domains (bold black texts in Figures 7b and 7c) are constrained by multiple independent datasets and observations (italicized red texts). In Figures 7b and 7c, the referenced borehole locations and associated data are provided in Supplementary Figures S3a-b and Supplementary Table S1.

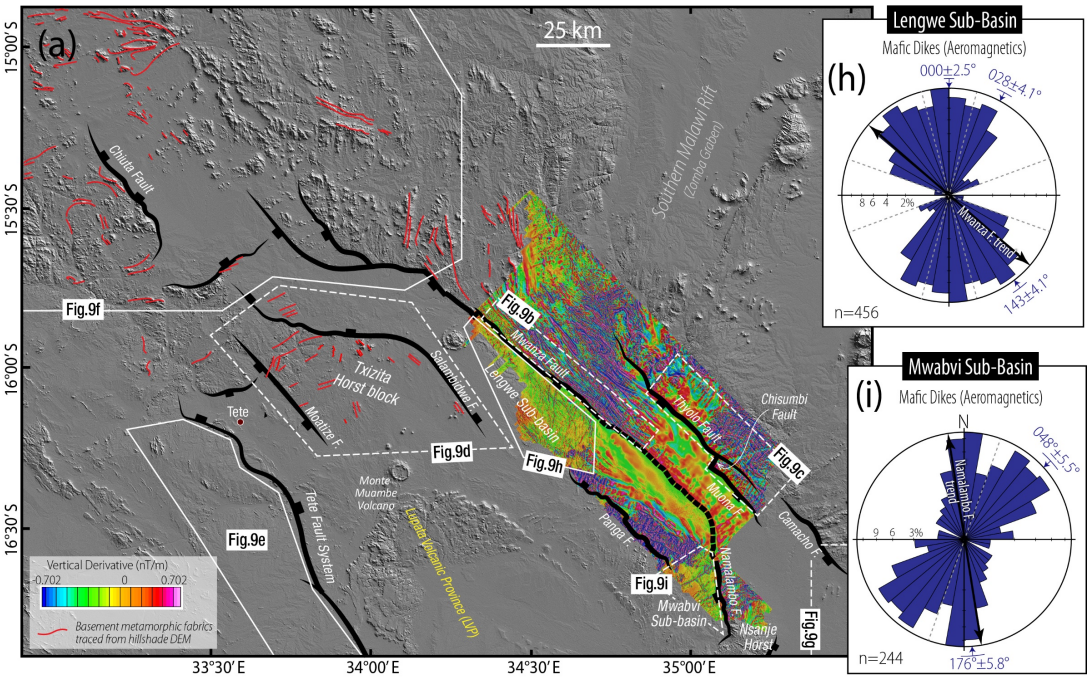
(a)
25 km
15°00'S
15°30'S
16°00'S
16°30'S
33°30'E
34°00'E
34°30'E
35°00'E
Chuula Fault
Southern Malawi Rift (Zomba Graben)
Fig.9f
Fig.9b
Mwanza Fault
Txizita Horst block
Salambidwe F.
Lengwe Sub-basin
Thyolo Fault
Chisumbi Fault
Fig.9c
Fig.9d
Fig.9h
Tete
Mwaiwe F.
Monte Muambe Volcano
Tete Fault System
Lupata Volcanic Province (LVP)
Panga F.
Mwabvi F.
Namalambo F.
Camacho F.
Fig.9i
Mwabvi Sub-basin
Nsanje Horst
Fig.9g
Fig.9e
Vertical Derivative (nT/m)
-0.702
0
0.702
Basement metamorphic fabrics traced from hillshade DEM
Lengwe Sub-Basin
Mafic Dikes (Aeromagnetics)
(h)
000±2.5°
028±4.1°
Mwanza F. trend
143±4.1°
n=456
Mwabvi Sub-Basin
(i)
Mafic Dikes (Aeromagnetics)
N
048°±5.5°
Namalambo F. trend
9 6 3%
n=244
176°±5.8°

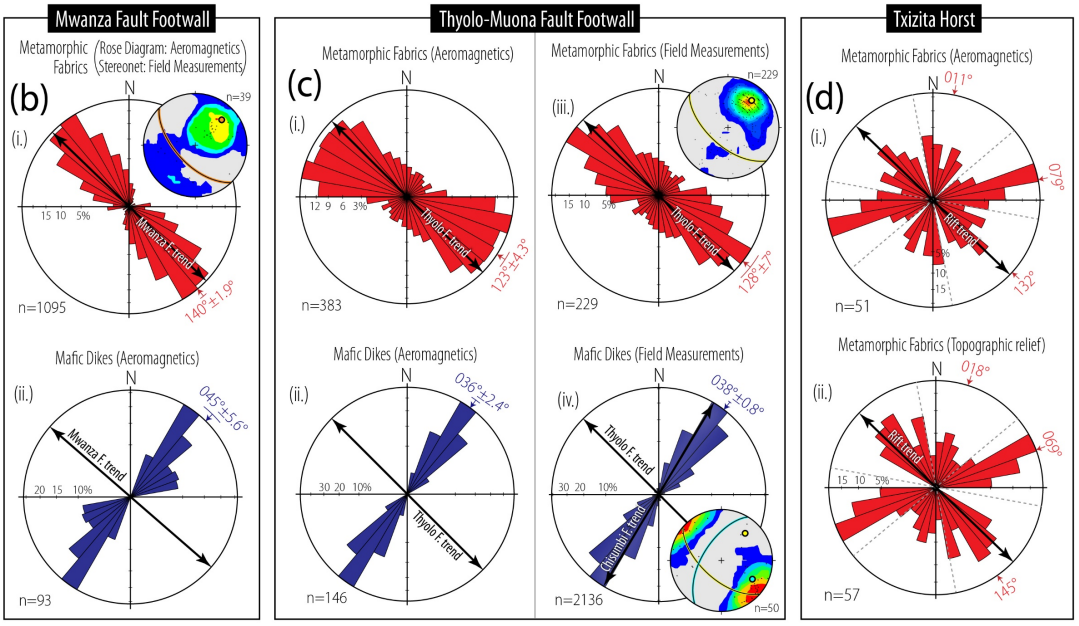
Mwanza Fault Footwall
Metamorphic Fabrics
Rose Diagram: Aeromagnetics
Stereonet: Field Measurements
(b)
(i)
N
n=39
15 10 5%
Mwanza F. trend
n=1095
140°±1.9°
Mafic Dikes (Aeromagnetics)
(ii.)
045°±5.6°
Mwanza F. trend
20 15 10%
n=93
Thyolo-Muona Fault Footwall
Metamorphic Fabrics (Aeromagnetics)
(c)
(i.)
12 9 6 3%
Thyolo F. trend
123°±4.3°
n=383
Metamorphic Fabrics (Field Measurements)
(iii.)
n=229
15 10 5%
Thyolo F. trend
128°±7°
n=229
Mafic Dikes (Aeromagnetics)
(ii.)
036°±2.4°
30 20 10%
Thyolo F. trend
n=146
Mafic Dikes (Field Measurements)
(iv.)
038°±0.8°
Thyolo F. trend
Chisumbi F. trend
n=50
n=2136
Txizita Horst
Metamorphic Fabrics (Aeromagnetics)
(d)
(i.)
011°
079°
Rift trend
132°
n=51
Metamorphic Fabrics (Topographic relief)
(ii.)
018°
069°
Rift trend
15 10 5%
145°
n=57

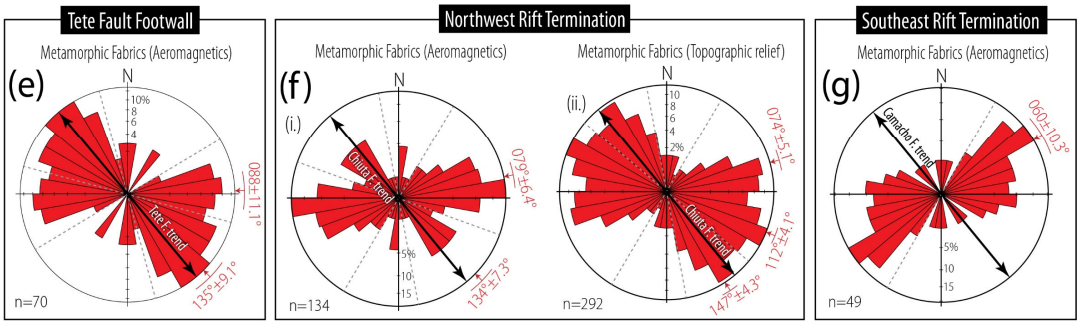
Tete Fault Footwall
Metamorphic Fabrics (Aeromagnetics)
(e)
N
10%
8
6
4
088°±11.1°
Tete F. trend
135°±9.1°
n=70
Northwest Rift Termination
Metamorphic Fabrics (Aeromagnetics)
(f)
(i.)
Chuula F. trend
079°±6.4°
5%
10
15
134°±7.3°
n=134
Metamorphic Fabrics (Topographic relief)
(ii.)
10
8
6
4
2%
074°±5.1°
Chuula F. trend
112°±4.1°
147°±4.3°
n=292
Southeast Rift Termination
Metamorphic Fabrics (Aeromagnetics)
(g)
N
060±10.3°
Camacho F. trend
5%
10
15
n=49

Figure 9. Structural trends of inherited basement fabrics (foliation) and syn-rift igneous dikes. (a) Shuttle Radar Topography Mission (SRTM) DEM hillshade map of the Shire Rift Zone overlaid with vertical derivative aeromagnetic map of the Malawi part of the rift. The red lines represent topographic expressions of basement fabrics around the rift (providing independent information on pre-rift basement fabrics, see Figs. 9d & 9f); (b - c) Azimuth-frequency distribution of basement metamorphic fabrics and mafic dikes along the footwall of (b) the Mwanza Fault, and (c) the Thyolo-Muona Fault System; (d - g) Frequency-azimuth distribution of metamorphic fabrics within the Txizita Horst block (9d), footwall of the Tete Fault System (9e), and the northwestern (9f) and southeastern (9g) rift terminations zones; (g - h) Frequency-azimuth distribution of mafic igneous dikes in the Lengwe (9h) and Mwabvi sub-basins (9i). Insets of stereographic projections (equal-area) represent poles to planes with 2 interval Kamb contours, and great circles with colored halos represent the Mwanza Fault plane (136°/60° in 9bi), Thyolo Fault plane (131°/60° in 9ciii-iv), and Chisumbi Fault (211°/60° in 9civ). The 60° dip of fault planes is obtained from previous field observation along the Thyolo Fault (Wedmore et al., 2020). In Fig. 9ciii, the rose and stereographic projection both consist of a combination of field measurements collected during our field visit (n=38) and those previously collected by the Malawi Geological Survey (n=191; Habgood et al., 1973). Whereas, in Fig. 9civ, although the rose plot includes a combination of our field measurements (n=50) and those in Habgood et al. (1973) (n=2086), the stereographic projection consists only of our field measurements as the dip of dikes were not reported in Habgood et al. (1973). Black dashed lines in rose plots represent frequency minima used for modal set grouping and calculation of circular vector mean for the modal sets.

~018° from topographic relief). The NE-trending fabrics appear to dominate most of the horst, whereas the NW-trending, which set is parallel to the rift trend, is primarily localized at the center and along the northeastern margin of the horst in the footwall of the Salambidwe Fault (Figures 4b, 5a, 9a).

4.3.3 The Tete Border Fault and Environs

Since the basement fabrics are poorly expressed in the topographic relief map (Figure 9a), we only obtain measurements of basement fabrics from the regional aeromagnetic grid (Figures 4b, 5a). The result shows a very prominent NW-SE trend (~135°) which is sub-parallel to the trend of the Tete Fault system (Figure 9e). However, we also observe a secondary set in the data which trends E-W (~088°) and is collocated with a kink in the trend of Tete Fault's trace (Figure 5a).

4.3.4 The Rift Termination Zones

At regional-scale, within the northwestern rift termination zone (i.e., vicinity of the Chiuta Sub-basin), the available aeromagnetic grid shows that the basement fabrics are

characterized by multimodal trends (Figure 9fi-ii) in which an ENE trend (~079° from aeromagnetics, ~074° from topographic relief) and NW-SE (134° from aeromagnetics, ~147° from topographic relief) trend are most prominent. The NW-SE fabric set is parallel to the trend of the Chiuta Fault (~137°). Whereas at the southeastern rift termination zone (SE tip of the Camacho Fault; Figure 9a), the basement is dominated by NE-SW -trending fabrics with a mean trend of ~060° (Figure 9g), which are sub-orthogonal to the Camacho Fault trend (~140°).

4.4 Syn-Rift Magmatic Structures in the Shire Rift Zone

Observations during our field visit (e.g., Figure 3b) and a compiled surficial geologic map of the SRZ (Figure 2) raise the need to explore the patterns and distribution of syn-rift diking and ring-shaped igneous structures that dominate the rift zone. The aeromagnetic fabric patterns and lineament 'types' observable in the filtered aeromagnetic grids include: 1) Broad clusters of parallel, elongate high-frequency, high-amplitude short-wavelength magnetic fabrics in exposed basement (Figure 4d), representing sub-vertical basement metamorphic foliation observable in field outcrops (Figures 3b-c); 2) Discrete cross-cutting lineaments of high-amplitude short-wavelength character enclosed by longer-wavelength magnetic-low anomalies, representing mafic igneous dike intrusions within sedimentary sequences in Lengwe and Mwabvi Sub-basins (e.g., Figure 4e) observable in exhumed Mesozoic syn-rift outcrops and boreholes (Habgood, 1963), among which lineament sets show different amplitudes indicative of different emplacement depths, here in described as "strong discrete lineaments, 'SDL'" (shallower dikes?) and "weak discrete lineaments, 'WDL'" (deep-seated dikes?); 3) Broad zones of high-amplitude mesh pattern fabrics in exposed basement (Figure 4f), representing metamorphic foliation overprinted by cross-cutting mafic dikes observable in field exposures (Figures S4a-c); 4) Broad zones of low-amplitude mesh pattern fabrics in intra-basinal areas of Quaternary-age sedimentary cover (Figure 4g), occurring as the buried lateral continuation of the metamorphic basement hosting cross-cutting mafic dikes (i.e. fabric type #3 buried beneath unconsolidated alluvial sediments); and 5) Broad zones of compact linear bands of chaotic high-amplitude high-

879 frequency magnetic fabrics (Figure 4h) collocated with exposed or shallowly buried
880 Mesozoic basaltic flows in the Mwabvi Sub-Basin (Figure 2; Habgood, 1963).

881 The basalt-related magnetic fabrics are cur and truncated by a system of sub-parallel
882 rectilinear abrupt gradients that correspond to faults (e.g., Panga Fault, observable in the
883 field and in topographic relief map; Figures 2, 4c). Also, the amplitude of the basalt-related
884 magnetic anomalies decreases northeastward towards the Mwanza Fault as the depth of
885 burial of the volcanic flows increases. Overall, in eastern SRZ in Malawi where high-
886 resolution aeromagnetic data is available (Figures 4a and 4c), we mapped and analyzed the
887 dike-related magnetic lineaments. In other parts of the rift zone where lower-resolution
888 aeromagnetic data is the only available subsurface data (Figures 4a and 4b), we show the
889 presence and distribution of prominent ring-shaped magnetic anomalies and describe their
890 associations with surface igneous complexes in the rift.

891

892 *4.4.1 Lengwe and Mwabvi Sub-Basins*

893 The high-resolution aeromagnetic data reveal the presence of a more complex
894 network of cross-cutting dike-related magnetic lineaments in the Lengwe Sub-basin than in
895 the Mwabvi Sub-basin (Figures S5a-b). The frequency-azimuth distribution of the Lengwe
896 dikes (Figure 9h) is multimodal with three dominant sets trending N-S (~000°), NNE-SSW
897 (~028°), and NW-SE (~143°). The NW-SE dike segments are generally sub-parallel to the
898 intrabasin faults, the Mwanza border fault, and the overall rift trend (Figure S5).

899 In the southern section of the Mwabvi Sub-basin where the dikes are observable, the data
900 (Figure 8i) shows only two dominant sets which include a N-S (~176°) and NE-SW (~048°)
901 trend. The N-S trending dike segments are parallel to the strike of the Namalambo Fault
902 representing the border fault in that part of the basin (Figure S5b). Whereas the NE-trending
903 dikes, some of which extend across the border fault, are parallel to the trend of the basement
904 fabrics in the Namalambi Fault footwall (LSZ and surrounding fabrics at the SE rift
905 termination zone; Figure 5a). Further, some of the NE dikes that extend across the
906 Namalambo Fault are collocated with the zone of burial of the northern tip of the Namalambo
907 Fault, and en-echelon transverse offsets of the fault beneath the Quaternary cover ('T' in
908 Figure S5b).

4.4.2 *Mwanza and Thyolo-Muona Border Fault Footwalls*

In the footwall of the Mwanza Fault, the dikes show a dominant (unimodal) NE-SW trend, ~045° (Figures 9bii, S4a-c). Similarly, on both the footwalls and hanging walls of the Thyolo-Muona Fault system, the dikes show a prominent unimodal trend of ~036° (Figures 9cii, 10a-b), consistent with field measurements in their footwalls (~038°; Figure 9civ and stereographic projection). Our field measurements (stereographic contours in Figure 9civ) show that in dip view, the dikes occur in a conjugate set with some dipping to the NW and others to the NE. Although the Thyolo and Muona Faults are sub-orthogonal to the dikes, the Chisumbi Fault (~031°) strikes parallel to the dikes and shows strong alignment in dip magnitude and direction with the NW-dipping dike set (see pole to Chisumbi Fault plane in Figure 9civ).

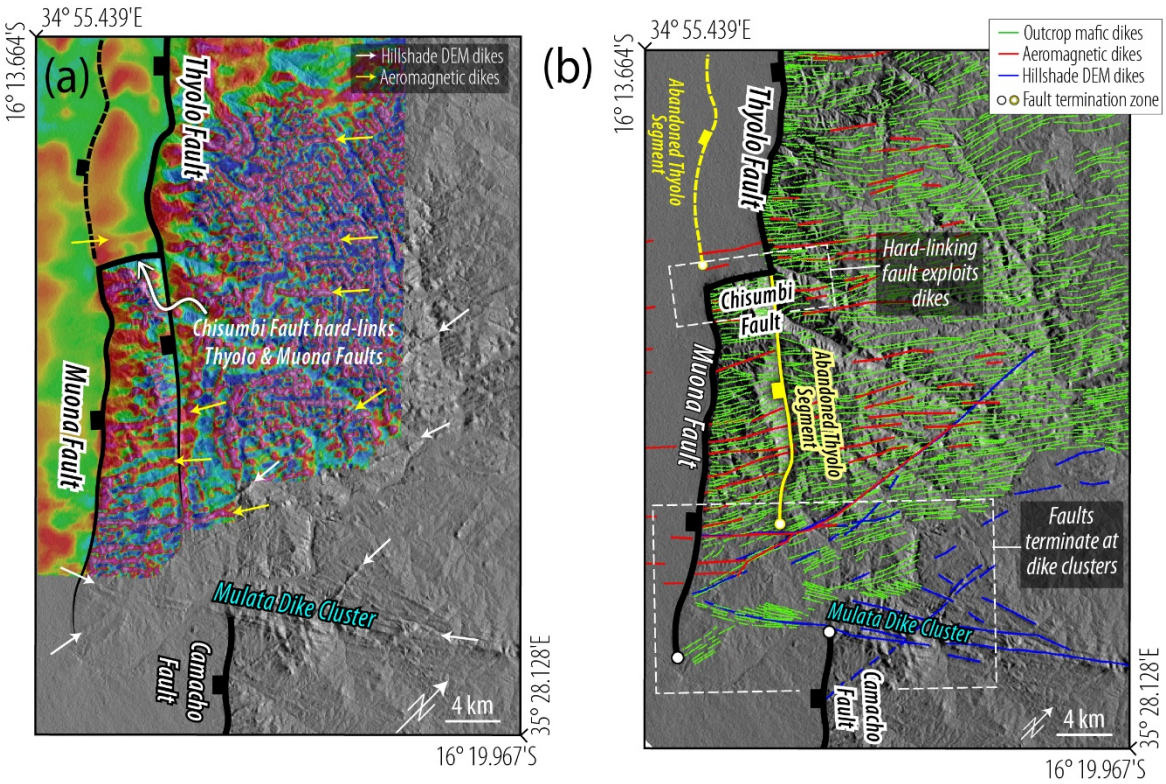

Figure 10. Relationships between the rift border faults and the early phase (RP1-RP2) mafic dikes. (a) Filtered aeromagnetic map (location: SE half of polygon "Fig. 9c" in Figure 9a) showing aeromagnetic dike lineaments (yellow arrows) and topographic expression of dikes (white arrows); (b) Map of same area in Figure 10a, showing the interpreted mafic dike aeromagnetic lineaments (red lines), SRTM hillshade dike lineaments (blue lines), and those from published field mapping (green lines; Habgood et al., 1963).

939 *4.4.3 Lupata Volcanic Province (LVP)*

940 The regional aeromagnetic grid shows that both the Monte Muambe Volcano (MV)
941 and Salambidwe Igneous Structure (SIS) are characterized by prominent ~10 km-wide ring-
942 shaped magnetic-high anomalies (Figure 4b). South of the Monte Muambe Volcano, we
943 identify several similarly-sized ring-shaped high-amplitude magnetic anomalies (with 7.5 –
944 19 km diameters) distributed over a distance of 140 km (Figures 4b and 5a). These ring-
945 shaped anomalies do not correspond to any distinct surface topographic feature. However,
946 the anomalies delineate a NW-trending belt along the rift axis.

947

948 **5 DISCUSSION**

949 **5.1 New Interpretation of the SRZ Architecture**

950 Although the broad geologic history of the SRZ has been previously identified
951 (Castaing, 1991), only the Lengwe, Mwabvi, and Lower Shire depocenters were
952 distinguished while the rest of the basin was referred to as the Middle Zambezi Valley
953 (Castaing, 1991, Chisenga et al., 2019). Thus, the detailed structure, rift basin
954 compartmentalization, and the associations with the phases of extension are not known. The
955 extent and distribution of fault-bounded Mesozoic and Cenozoic sedimentary and
956 volcaniclastic deposits in the Shire Rift (Figure 2) represent a multiphase rift zone with
957 compartmentalization (Figure 5b) that is facilitated by complex brittle and magmatic
958 deformation (Figure 8). Based on the integration of surficial geology (Figure 2) and
959 structural interpretations from filtered aeromagnetic datasets, we identified seven
960 structural domains within the basin, which include the Lower Shire, Mwabvi, Lengwe, Monte
961 Muambe, Moatize, Chiuta, and Lupata Sub-Basins (Figure 5b).

962 Based on the presence of basement-sedimentary magmatic intrusions, volcanic
963 deposits, and timing of magmatic activities in the SRZ, we characterized the sub-basins into
964 magmatic and non-magmatic categories. Considering that the Lupata Sub-Basin houses the
965 Lupata Volcanic Province (LVP) where multi-phase rejuvenation of widespread intra-rift
966 volcanism localized during RP1-RP2, we suggest that this sub-basin likely hosts some of the
967 richest information on multiphase early-stage magmatic rifting, yet it remains poorly
968 understood. Also, the spatial extents of syn-rift sequences across the SRZ (Figures 2) suggest

969 that the Lengwe, Mwabvi, Moatize, and Monte Muanbe Sub-basins were established and
970 most active during RP1 (Figure 11a). Late-RP1 magmatic plumbing of the rift appears to be
971 basin-scale (Castaing, 1991). However, RP2 tectonic activities largely involved the focusing
972 of intra-rift volcanism in the LVP, the Salambidwe area of the Lengwe Sub-basin, and
973 localization of off-rift magmatism outboard of the evolving rift (Chilwa Alkaline Province,
974 CAP; Figures 2, 8, 11b).

975

976 *5.1.1 Possible Cenozoic Establishment of the Lower-Shire and Chiuta Sub-Basins*

977 As is the case in many onshore basins in East Africa, the lack of surface-to-basement
978 wells limits the understanding of the spatiotemporal rift propagation at the segment scale. A
979 similar challenge arises here in the SRZ, where available legacy boreholes only sampled
980 shallow depths in the Chiuta and Lower Shire Sub-basins. However, based on the most up-
981 to-date compilation of surface and subsurface data on the SRZ, we infer the most probable
982 rift history of the two sub-basins with the most widespread accumulations of RP3 deposits.

983 Bloomfield (1958), Cooper and Bloomfield (1961), and Habgood (1963) documented
984 the presence of ~1.2 km-wide hydrothermal alteration zone along the escarpment and
985 footwalls of the Mwanza Fault and Namalambo Fault. The alteration zones are characterized
986 by unbroken silicic and calcite hydrothermal veins with associated epidote and pyrite
987 mineralization, and they preserve evidence of multiple episodes of fluid alteration
988 (Bloomfield, 1958). Along the Namalambo Fault zone, the veins crosscut both the
989 Precambrian basement and brecciated RP1 diabase intrusions (Bloomfield, 1958). Based on
990 the observed cross-cutting relationship and the large-scale 'unbroken' structure of the veins,
991 this pervasive hydrothermal event has been interpreted to have occurred during the Late
992 Cretaceous rifting activity (RP2). However, field observations along the Thyolo-Muona Fault
993 zones show no evidence of fluid alteration (this study, and others: Williams et al., 2019;
994 Wedmore et al., 2020), suggesting that the fault zones did not undergo the same
995 hydrothermal events observed along the Mwanza and Namalambo Faults. These
996 observations suggest that the Thyolo-Muona Fault System was likely not established until
997 the RP3.

998 The absence of Mesozoic volcanic rocks in the hanging wall of the Thyolo-Muona
999 border fault suggests that the Lower Shire Sub-basin was most likely not established as a
1000 major depocenter during the magmatic RP1-2 rift phases (Figures 7a-c, 11c). Also, in the
1001 other on-shore Eastern Africa rift basins that accommodated RP1-RP2 rifting and have been
1002 reactivated in the Cenozoic, outcrops of the Mesozoic syn-rift units have been documented
1003 along their uplifted flexural margins (e.g., Rukwa Rift, Luangwa Rift, Northern Malawi Rift;
1004 Bennett, 1989; Ring 1995; Delvaux, 2001; Kolawole et al., 2018; Daly et al., 2020). However,
1005 in the uplifted flexural margins of the Chiuta Sub-basin and hanging walls of the Thyolo-
1006 Muona Fault, outcrops of RP1-RP2 sedimentary rocks are absent. Also, the magnetic anomaly
1007 pattern in the hanging walls of the Thyolo and Muona Faults (see Figure 7a) primarily
1008 exhibits long-wavelength anomalies of buried metamorphic fabrics crosscut by mafic dikes,
1009 both confined to the crystalline basement beneath the sedimentary cover (Figures 4f-g).
1010 Whereas, in the hanging wall of the Mwanza and Namalambo faults where RP1-RP2 syn-rift
1011 sequences are widespread, the magnetic fabric pattern is dominated by discrete magnetic-
1012 high short-wavelength lineament anomalies of mafic dikes that intruded the syn-rift
1013 sedimentary sequences (Figures 4e, S5a-b; also see field and borehole observations in
1014 Habgood, 1963; Castaing et al., 1991). In essence, the Thyolo-Muona fault hanging wall lacks
1015 the presence of sedimentary sequences with intruded mafic dikes.

1016 The modeled depth-to-crystalline-basement in the Chiuta Sub-basin and Thyolo-
1017 Muona Fault hanging wall (Figures 6a-b) generally shows <1.5 km depth, which is consistent
1018 with basement depths in the nearby southern Malawi Rift (maximum of 1.6 km) where an
1019 absence of Mesozoic rifting has been similarly inferred (Scholz et al., 2020; Williams et al.,
1020 2021). At regional scales, geodetic stretching rates generally decrease towards the euler pole
1021 of plate rotation, such that within a sub-region of contemporary rifting such as the Shire Rift
1022 Zone and Southern Malawi Rift, crustal stretching rates can be assumed to be relatively
1023 uniform spatially (~2.2 mm/yr; Stamps et al., 2018; Wedmore et al., 2021). Thus, if both the
1024 southern Malawi Rift and Lower Shire Graben have experienced tectonic extension for the
1025 same length of time, the maximum throws on the active border faults should be relatively
1026 similar, assuming a uniform time-averaged crustal stretching rates across the sub-region.
1027 Therefore, the similarity of maximum border fault throws in southern Malawi Rift to those

of the Chiuta Sub-Basin and Thyolo-Muona Fault hanging wall, given by maximum depth-to-basement along the border faults, suggests that the three areas are likely coeval.

Dixey (1925) also noted the absence of RP1 and RP2 syn-rift sediments in the Lower Shire Sub-basin (i.e., in the area between Mwanza Fault and Thyolo-Muona Fault) and speculated on ~400 m Jurassic-age uplift event (immediately after RP1) and additional ~1.2 km Late Miocene-age localized uplift event (after RP2) within the sub-basin that could have led to the erosion of both the RP1 and RP2 syn-rift deposits immediately after each rift phase. These speculations are problematic considering that 1) the suggested magnitude of post RP1 uplift implies that the Lower Shire area (i.e., Mwanza Fault's footwall) did not experience significant tectonic subsidence during RP1, and 2) results from thermochronology studies in the area does not support the occurrence of a localized uplift, but rather a regional-scale Paleogene tectonic uplift (Daszinnies et al., 2008; Ojo et al., 2020 *in review*). The studies show the occurrence of regional Eocene-age uplift associated with the initiation of East African Rift System (Daszinnies et al., 2008) and Late Cenozoic footwall uplift along the Thyolo Fault (i.e., RP3 rift border faulting; Ojo et al., 2020 *in review*).

Coal deposits are known to preserve excellent records of maximum paleotemperatures that they have been exposed to (e.g., Hunt et al., 2002; Singh et al., 2007). Geochemical analyses of the Karoo-age (RP1) coal seams of the Lengwe-Mwabvi Sub-basins show approximate carbon content of 75.7 % and volatile matter of ~25 % on a dry ash free basis (Habgood, 1963). These values indicate orthobituminous coals of high to medium volatile bituminous rank, corresponding to victrinite reflectance of ~0.9 - 1.5 % (Hunt et al., 2002; Suárez-Ruiz & Crelling, 2008). Assuming an average geothermal gradient (25-30 °C/km in continental crust) and normal burial-and-exhumation paths, these RP1 coal-rich units would have been buried to about ~3 - 4 km depths to attain the estimated thermal maturity level (Bjorlykke, 1989) prior to exhumation. However, such a simple burial-and-exhumation history cannot be assumed here considering the RP1 and RP2 magmatic events and associated intrusions into the coal-rich syn-rift sequences (Habgood, 1963; Figs. S5a-b) and the strong thermal maturation effects of such extraneous heat sources on coal deposits (e.g., Stewart et al., 2005; Singh et al., 2007). Therefore, we infer that the exhumed RP1 units

in the Lengwe-Mwabvi Sub-basins (adjacent to the Lower Shire Sub-basin) were likely only buried to depths much shallower than 4 km prior to their Cenozoic exhumation.

We acknowledge that it is still possible that the current locations of the Chiuta Sub-basin and Thyolo-Muona Fault's hanging wall area hosted syn-rift Mesozoic depocenters that were eroded off at sometime between the Cretaceous and Cenozoic rift phase. However, such depocenters may have been significantly smaller and shallower (diffused rifting?) than those hosted and preserved in the other sub-basins with widespread outcrops of RP1-2 deposits: Lengwe, Mwabvi, Moatize, Monte-Muambe, and Lupata Sub-basins. Therefore, we argue that that the Chiuta Fault and the Thyolo-Muona Fault Systems were likely not established as major syn-rift depocenters along the SRZ until the RP3. Thus, it is still possible that isolated pockets of small RP1-RP2 sedimentary deposits may be preserved at the deepest parts of these major RP3 sub-basins, but would require a future basement-penetrating drilling campaign to confirm. Also, we emphasize that unlike the RP1-RP2 strain accommodation in the SRZ that recorded pronounced magma-assisted rifting, the RP3 strain accommodation in the rift zone is not magma-assisted.

5.2 Pulsed Rift Propagation in the SRZ: Multiphase Strain Migration and Sub-Basin Abandonment

The absence of major RP1-RP2 depocenters in the Chiuta Sub-basin and Thyolo-Muona Fault's hanging wall suggests that the RP1-RP2 rift deformation and subsidence were largely confined to the region bounded by the Mwanza-Namalambo Fault to the northeast and the Tete Fault to the southwest. To the northwest, the RP1-RP2 rift bifurcates and appears to have terminated at or near the intersection of the rift with the Senangoe Shear Zone. To the southeast, the rift-bounding Namalambo Fault also terminates at the Lurio Shear Zone. However, the localization of the Chiuta Sub-basin to the northwest of the Sanangoe Shear Zone in RP3 suggests that the Cenozoic rifting in the SRZ recorded a resurgence of lateral along-trend propagation of the rift basin. The absence of RP3 tectonic activity in the LVP and surrounding sub-basins suggests that this previously active magmatic domain of the rift was largely abandoned after RP2, and strain has migrated further

northwest and east/northeast of the basin. The RP3 rift-orthogonal strain migration into the margin of the older basin led to the development of the Lower Shire Graben.

This sequence of temporal rift evolution describes a pulsed pattern of lateral rift propagation in which continuous lateral propagation of the tip of an active rift is stalled for a considerable period, after which rift lengthening resumes (Courtillot 1982; Van Wijk and Blackman, 2005). However, questions arise as to the forcing mechanism behind the large-scale abandonment of the RP1-RP2 basin and rift-orthogonal strain migration into the northeastern rift margin. Strain migration during multiphase rifting is not uncommon in the tectonic records of rifted continental margins and failed continental rifts (e.g., Braun, 1992; Bell et al., 2014; Fazlikhani et al., 2020). In the SRZ, the Mesozoic phases of rifting were accompanied by voluminous basaltic magmatism (Figures 2 and 11; Castaing et al, 1991), and gravity modelling reveal the possible presence of sub-crustal intrusive bodies beneath the SRZ-related RP2 igneous provinces (Njunju et al., 2019b).

Therefore, an explanation for the basin abandonment and strain migration could be a possible strengthening (healing) of the crust and lithospheric mantle beneath the early-phase sub-basins, facilitated by a prolonged inter-rift period between RP2 and RP3 after the RP1-RP2 magma-assisted crustal thinning. This inference is supported by lithospheric-scale rift models (e.g., Braun, 1992; Naliboff and Buiter, 2015). Braun (1992) argued that the absence of RP3 reactivation in the RP1-RP2 rift basins flanking the northern Malawi Rift (Ruhuhu and Maniamba Rifts; Figure 1a) is due to inter-rift lithospheric healing, such that relatively unstretched regions of the mobile belts served as strain concentrators in the RP3. The integrated crustal strength of the magmatic RP1-RP2 rift zone may likely have surpassed that of the surrounding areas (Naliboff and Buiter, 2015), such that the initiation of Cenozoic crustal stretching (RP3) favored the migration of strain into the surrounding areas. We note that although other magmatic RP1-2 rifts in the region such as the Zambezi Rift also show a similar style of large-scale post-RP2 abandonment, the border faults of the Luangwa Rift are experiencing RP3 reactivation (Daly et al., 2020). However, it is also not yet clear if inter-RP2-3 lithospheric healing also controlled the absence of resurgent magmatic rifting in the RP3 along the SRZ, considering that the basin was largely magmatic in the previous phases of extension.

5.3 Inheritance of Weakening Structures: Strain Localization Through the Exploitation of Intra-Basement Weak Zones

5.3.1 Early-Phase (RP1) Border Faulting

If the Mwanza-Namalambo and Tete Faults are the main Mesozoic border faults of the SRZ, based on the present-day surface locations of the faults and exposures of syn-rift basin-fill, we estimate that the RP1 basin is a NW-trending rift basin that bifurcates northwestwards into two 20-25 km-wide branches, covering a total of ~17,299 km^2 areal extent over a length of ~200 km (Figures 5b, 11a). The branches are also confined by 'inner' border faults, Moatize, and Salambidwe Faults, which juxtapose the rift-fill against the pre-rift basement of the Txizita Horst (Figure 5d).

Along the eastern rift shoulder, the Mwanza Fault's strike and dip show strong alignment with those of the underlying pre-rift basement metamorphic fabrics (Figures 9b, 11a). In the northern Lengwe Sub-basin where the Mwanza Fault rotates counter-clockwise, field observations in Barr and Brown (1987) show that the fault is collocated with- and follows the easternmost segment of the crustal-scale Precambrian Sanangoe Shear Zone (SSZ). Likewise, the Salambidwe Fault is parallel to the trends of the basement fabrics (Figures 4a, 9a). However, to the SE, the N-trending Namalambo border fault cuts across the NE-trending basement fabrics of the Lurio Shear Zone (LSZ), except for its southernmost tip which rotates clockwise and follows the trend of the basement fabrics (Figure 5a; Bloomfield, 1958). We note that the southernmost part of the Namalambo Fault bends into a NE trend which parallels the LSZ (Figures 4b, 5a). Along the western rift shoulder, the northernmost sections of the Tete Fault trend parallel to aeromagnetic basement fabrics (Figures 4b and 9e), which is consistent with observations in published geologic maps (Choubert et al., 1988). Whereas, the Moatize Fault, the inner border fault of the Moatize rift branch, appears to crosscut the metamorphic basement fabrics (Figures 4b, 5a, 9a). Overall, based on these observations, we suggest that that the RP1 eastern border fault (Mwanza Fault) exploited the pre-rift basement fabrics along most of its length, whereas the western border fault (Tete Fault) partially exploited the basement fabrics.

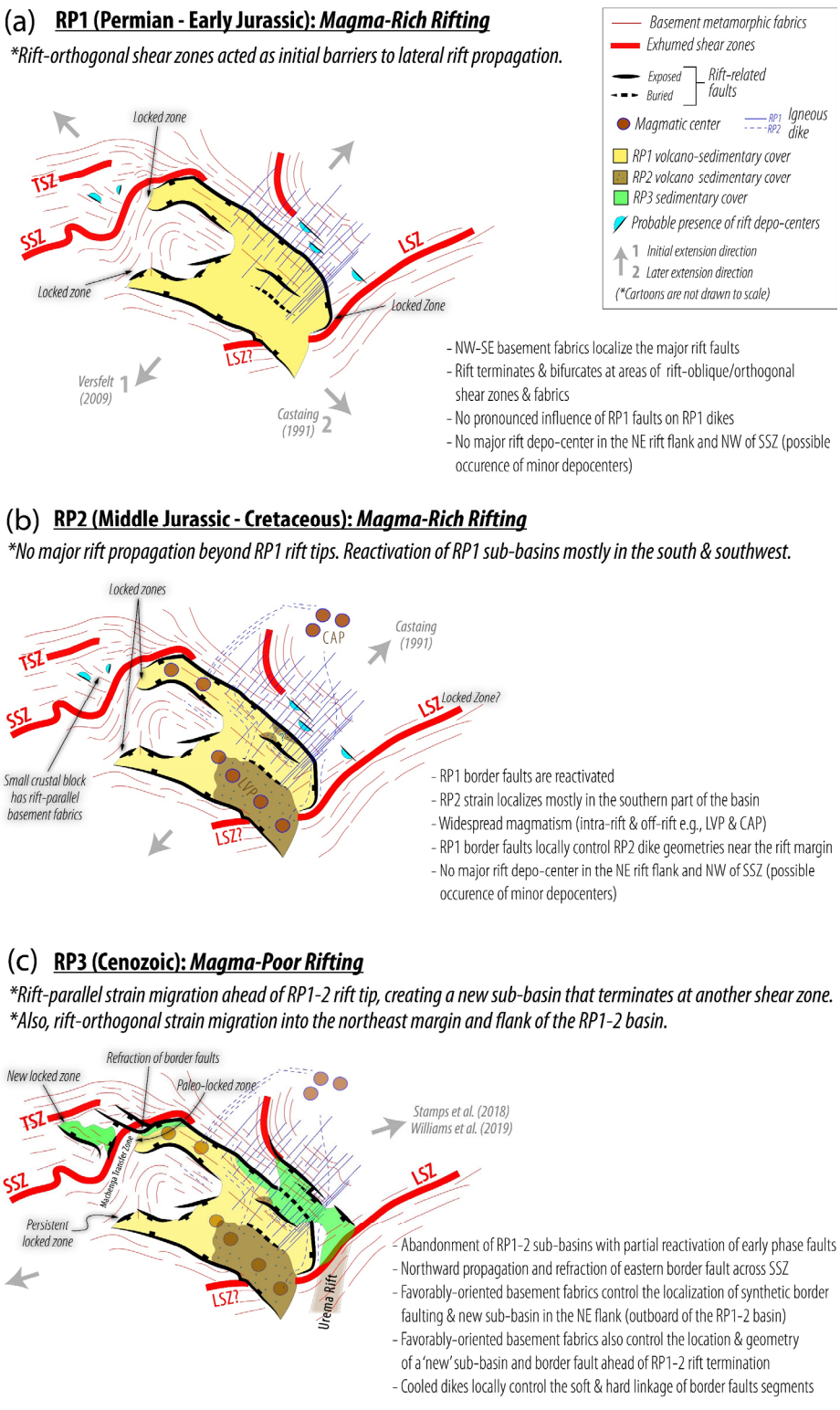

Figure 11. Cartoons summarizing the multiphase evolution and strain migration in the Shire Rift Zone, based on observations in this study. LSZ: Lurio Shear Zone, MDC: Mulata Dike Cluster, SSZ: Sanangoè Shear Zone.

The large-scale alignment of the early-phase border faults with those of the underlying pre-rift basement metamorphic fabrics suggests that the border fault likely exploited the basement fabrics during rift initiation. Due to limited field access, we are only able to assess the 3-D component of the alignment in the Malawi extension of the SRZ. However, our observations along the Mwanza Fault escarpment show a correspondence between the strike, dip magnitude, and dip direction of the basement fabrics with those of the border fault. The gneissic basement foliation along the SRZ border faults constitute planes of mechanical weakness that was exploited by brittle deformation during the early-rift extension (e.g., Donath, 1961; Youash, 1969; Ranalli and Yin, 1990; Morley, 1999, 2010). However, the inferred NW-SE regional extension direction for RP1 (Castaing, 1991) is not compatible with the development of NW-trending faults, and even less likely in a crust with NW-trending pre-rift mechanical anisotropy (Youash, 1969; Morley, 1999). Although Castaing (1991) inferred strike-slip kinematics for the RP1 rifting, the rift structure lacks the map-view rhombic geometry or associated Reidel pattern faulting that is typical of strike-slip and transtensional basins.

Thus, we argue that it is more likely that the SRZ first accommodated a NE-oriented tectonic extension during early RP1, and in late RP1, the rotation of extension direction into a NW-SE direction facilitated an oblique-normal or strike-slip reactivation of the early rift border faults (Figure 11a). This is supported by the Lower Jurassic age (late RP1) of the magmatic diking of the rift (Habgood, 1963) upon which the inference of NW-SE-oriented $\sigma 3$ was based. We infer that the basement fabrics could have been favorably-oriented for brittle exploitation by the early rift border faults within the NW-directed early-RP1 extension direction. Such favorably-oriented planes of mechanical weakness in the basement have been noted to facilitate the localization of the early-rift border faults in other Karoo rifts that were coeval with the SRZ (e.g., Rukwa and Luama Rift; Wheeler and Karson, 1994; Kolawole et al., 2021a). This interpretation of basement inheritance is consistent with previous observations in different parts of the SRZ (e.g., Cooper and Bloomfield, 1961; Castaing, 1991; Williams et al., 2019; Wedmore et al., 2020a) and other rift segments of the East African Rift System (Kinabo et al., 2007; Morley, 1999, 2010; Wheeler and Karson, 1989, 1994; Kolawole et al., 2018; Heilman et al., 2019).

5.3.2 Later-Phase (RP3) Border Faulting

The Cenozoic (RP3) sub-basins in the SRZ: the Lower Shire and Chiuta Sub-basins, developed in the hanging walls of border faults with prominent escarpments and along which the RP3 sedimentary rift-fill is thickest (Figures 5c-e, 6a-b). However, we note that although the southern sections of the Mwanza Fault that are buried beneath Quaternary sediments (dashed Mwanza fault trace in Figure 8) do not appear to be active in the current rift phase, the northern sections of the fault have been partially reactivated. This partial reactivation is inferred from the presence of narrow zones of Quaternary sedimentary cover along the northern Mwanza Fault (see Figure 3).

The Thyolo, Muona, Chisumbi, and Camacho faults define distinct segments of a system of synthetic border faults along the Lower Shire Graben (Figures 8, 10a-b). All three segments show side-stepping geometries among which the Thyolo and Muona segments are hard-linked by the Chisumbi segment but soft-linked with the Camacho Fault (Figures 6a-b). The northwesternmost segment, the Thyolo Fault, side-steps basinward to the right and overlaps with the Muona Fault, which extends ~27 km SE and side-steps to the left towards the hinterland where it overlaps with the Camacho Fault (Figure 8). The Camacho Fault terminates to the SE near the NE-trending Precambrian Lurio Shear Zone (LSZ) where the basin geometry rotates from the NW-SE trend into a N-S trending graben and transitions into Urema Graben (Figure 5). These faults are active in the current regional normal faulting stress field (Williams et al., 2019). The large-scale alignment of the Thyolo and Muona faults with the basement metamorphic fabrics suggests that these border fault segments likely localized by exploiting of the basement fabrics at depth (Hodge et al., 2018). It has been proposed that the Thyolo border fault likely exploited a Precambrian terrane boundary that terminates the Unango Complex to the south (Wedmore et al. (2020a). This interpretation of structural inheritance is further supported by the non-optimal orientation of the NW-trending basement fabrics to the current ENE-trending regional extension direction (Williams et al., 2019).

However, we also find evidence of possible control of rift-orthogonal intra-basement structures on the hard- and soft-linkage, and termination of the side-stepping Lower Shire

1236 border fault segments. In the hanging wall of the Thyolo Fault, the aeromagnetic grids reveal
1237 a magnetic gradient defining a northwestward continuation of the Muona Fault beneath the
1238 Quaternary sediments (Figures 10a-b). This buried Muona Fault continuation is truncated
1239 and separated from the exposed southeastern section of the fault by the NE-trending
1240 Chisumbi Fault which physically connects the exposed Muona Fault to the Thyolo Fault
1241 (Figures 10a-b). Similarly, the Chisumbi Fault defines the boundary between the
1242 northwestern section of the Thyolo Fault hanging wall with Quaternary cover from the
1243 southeastern section where there is no sedimentary cover (Figure 2). Essentially, the
1244 Chisumbi Fault breached the relay zone between the Thyolo and Muona Faults sometime
1245 after the faults had been established, and hard-linked them together (also see Wedmore et
1246 al., 2020a). However, our field data on the strike and dip of the cooled RP1 mafic igneous
1247 dikes along the rift shoulder (Figure 9civ) shows an alignment of the Chisumbi Fault with the
1248 intra-basement dikes, suggesting that the hard-linkage of the border fault segments was
1249 facilitated by the brittle exploitation of the cooled intra-basement dikes (Figure 10b). The
1250 mechanical contrast created by the mafic dike contacts could have localized the hard-linking
1251 fault segment. This interpretation is also consistent with a recent field study of the Thyolo-
1252 Chisumbi-Muona Fault (Wedmore et al., 2020a).

1253 Additional observation of possible brittle deformation localized by the cooled early-
1254 phase dikes is shown in the filtered aeromagnetic images along the northern and southern
1255 boundaries of the buried ~60 km-long southern section of the Mwanza Fault. The images
1256 reveal transverse truncation and offset of the NW-trending fault along the contacts of the
1257 NE-trending dike lineaments ("T" in Figures S4c and S5b). These truncations are more
1258 pronounced at the northern tip of the Namalambo Fault where the dikes appear to align with
1259 and follow the NE-trending basement fabrics along trend (Figure S5b). We interpret that the
1260 truncating structures are shallow transverse faults that exploited mechanical anisotropies
1261 within the cooled dike swarms (e.g., dike contacts), consistent with observations elsewhere
1262 in the North Sea Rift (Phillips et al., 2017). These transverse faults appear as oblique-normal
1263 faults that cut the pre-existing well-developed border faults in RP3 (Figure S5b), or served
1264 as side-stepping faults (Figure S4c), to accommodate the subsidence of the Lower Shire
1265 Graben along the hanging walls of the RP3 border faults as strain has now migrated away

from the older Mwanza-Namalambo border fault. Thus, we suggest that the RP3 subsidence and burial of the southern Mwanza Fault, a major long-lived RP1-RP2 border fault of the SRZ is related to both the subsidence of the Thyolo-Muona Fault and Panga Fault hanging walls and subsidiary faulting along the transverse faults. However, we do not rule out a possibility of reactivation of the buried Mwanza Fault segment prior to and after its burial.

At the distal northwest, major border faulting along the SRZ is defined by the Chiuta Fault (Figures 5a and 6b) where the fault and its sub-basin developed within a zone of NW-trending basement fabrics (Figures 4b and 5a). The alignment of the Chiuta Fault with the bounding basement fabrics (Figures 4b, 9a, and 9f) suggests that the nucleation of the fault also exploited the basement fabrics.

5.4 Inheritance of Resisting Structures: Transient Barriers to Continuous Lateral Rift Propagation in the Crust

5.4.1 Rift-Orthogonal Intra-Basement Shear Zones

Based on basement field studies in the northwestern parts of the SRZ (Barr and Brown, 1987; Evans et al., 1999), we suggest that the large-scale bifurcation structure of the SRZ and geometry of its branches are influenced by the crustal-scale ENE-trending Precambrian Sanangoè Shear Zone (SSZ; Figures 1a-b, and 5a-b). Filtered aeromagnetic grids show that the southwestern branch of the SRZ (i.e., the Moatize Sub-basin) terminates at a zone of ENE-trending metamorphic fabrics corresponding to gneisses, schists, and diabase dikes of the underlying Proterozoic basement terrane (fabrics in the northern parts of Txizita Horst in Figures 4b and 9a). Within this zone of termination, the northeastern branch rotates counter-clockwise to the west and the Mwanza border fault splays into two NW-trending segments near its intersection with the SSZ (Figure 5a). Within this region of border fault splay, the basement is exposed, defining a termination of the RP1-RP2 graben along the northeastern branch, and we here-in refer to as the 'Machenga Transfer Zone, MTZ' (see location in Figures 5a-b). Although the Chiuta Sub-basin is localized to the north of the MTZ, its southern bounding fault is oriented ENE-WSW, following the trend of the SSZ (Figure 5b).

Thus, we infer that the initial termination and stagnation of the RP1-RP2 SRZ rift tip was controlled by the SSZ which possibly represented a mechanical barrier to continued

early-phase lateral propagation of the rift zone. Also, we note that although in RP3 tectonic strain migrated further northwest of the SSZ, represented by the Chiuta Sub-basin, the RP3 sub-basin also terminates near another zone of ENE-trending basement fabrics with a plunging ductile shear zone (Techigoma Shear Zone, TSZ; Figures 4b, 5a, and 5a inset). Furthermore, we suggest that the establishment of the Chiuta Sub-basin was facilitated by strain localization within an isolated crustal block of NW-trending basement fabrics that is located ahead, but proximal to and colinear with the earlier established RP1-RP2 rift zone. To the southwest, the RP1-RP2 border fault system either terminates at the NE-trending Lurio Shear Zone (Namalambo Fault) or rotates and forms a kink geometry at its intersection with the shear zone (Tete Fault System) (see 'NF ' and 'TFS' geometries in Figure 5a). We also note that the southern tip of the Namalambo Fault rotates clockwise into the NE trend of the shear zone. These exhumed intra-basement shear zones are crustal-scale boundaries between different basement terranes (Barr and Brown, 1987; Kröner et al., 1997; Evans et al., 1999; Bingen et al., 2009). These observations lead us to infer that the rift-orthogonal crustal-scale intra-basement shear zones acted as mechanical barriers that influenced the initial termination of the Shire Rift Zone during RP1 and RP2, and again terminated the newly localized RP3 sub-basin at the northwestern rift tip during the current phase of extension (Figures 11a-c). In essence, these shear zones influenced the pulse pattern of multiphase lengthening of the rift zone.

The NE trend of the shear zones is misoriented for brittle reactivation in the current regional ENE-extension direction, and this 'misorientation' of the mechanical anisotropy created by the shear zones may have damped the stress concentration at the propagating rift tips. However, we suggest that the lateral variation of crustal strength across the shear zones, and the broader rheological domain around the shear zones (e.g., up to 8 km wide zone of metamorphic deformation and gabbroic intrusions along the SSZ) most likely influenced the temporary stagnation of rift tips near the shear zones. This interpretation is consistent with models in Courtillot (1982) which demonstrated that propagating rift tips can become stagnated at strong ribbons of the crust referred to as 'locked zones'. Van Wijk and Blackman (2004) further showed that the lateral propagation of a rift tip is stalled within strong pre-

rift continental crust, such that during the stall phase, shear stresses progressively build up near the rift tip to facilitate a later resumption of lateral rift propagation.

In the SRZ, the counterclockwise rotation and splaying of the Mwanza border fault across the SSZ can be interpreted to represent refraction of the propagating border fault during the resumption of rift propagation in RP3. This interpretation is consistent with observations of normal fault splaying across misoriented crustal terrane boundaries along the path of lateral propagation of rift zones in the Great South Basin, New Zealand (Phillips et al., 2019b). Numerical models also demonstrate the temporary stagnation of propagating rift tips at terrane boundaries that are rift-orthogonal and bound terranes of contrasting crustal strength (Phillips et al., 2021). In addition, observations in other areas of early-stage continental rifting show that rift zones and their bounding faults terminate at major rift-oblique/orthogonal basement shear zones, for example, the termination of the Okavango Rift at the Sekaka Shear Zone (Kinabo et al., 2007), and the termination of the Rhino Rift at the Aswa Shear Zone (Figure 1a; Katumwehe et al., 2015; Kolawole et al., 2021b). Another possible example is the termination of the southern Main Ethiopian Rift at a rift-oblique basement terrane (Kounoudis et al., 2021).

5.4.2 Cooled Early-Rift Mafic dikes

In addition to the larger scale influence of intra-basement shear zones on rift termination, we also note that the cooled early-phase (RP1) magmatic plumbing structures of the basement beneath the SRZ may have influenced the arrangement and termination of the later phase (RP3) border fault segments. The cooled early-phase dikes did not only facilitate the hard-linkage, it appears that the dikes also facilitated the soft-linkage of the border fault segments in the Lower Shire Graben (Figures 10a-b). Both the Thyolo and Muona Fault segments terminate to the southeast at a zone of conjugate-pattern dike clusters consisting of N and NW-trending dike sets (see dike clusters in Figures 10a-b). Likewise, the western tip of the Camacho Fault terminates at the Mulata Dike Cluster. We interpret that the inherited early phase dikes posed mechanical barriers to the lateral propagation of each RP3 border fault segment, resulting in the nucleation of multiple synthetic border fault segments that are soft-linked across the zone of conjugate dike cluster.

This may also imply that at this initial stage of development, the maximum lengths of the fault segments are delimited by the inherited cooled dikes.

In summary, during the pulsed or episodic propagation of a rift segment, inherited intra-basement strength anisotropies can act as both strain-localizing and strain-inhibiting tectonic elements within the lithosphere. We suggest that these mechanisms play important roles in the evolution of continental rift segment architecture during the early stages of continental extension.

6 CONCLUSIONS

We investigated the large-scale architecture and evolution of the Shire Rift Zone (SRZ) over the three phases of tectonic extension (RP1, RP2, and RP3) that are recorded in the basin. We compiled and integrated all available surface and subsurface datasets to better understand the pre-rift basement structure, major syn-rift depo-centers (sub-basins), the border fault structure, and their spatiotemporal distribution. Our results show that although the SRZ is characterized by seven major sub-basins, the RP3 (Cenozoic) sub-basins were activated at later phase of rifting. Overall, among the seven sub-basins, five are magmatic (deposition of volcanics and/or igneous intrusion in sedimentary units) and two are non-magmatic. Thus, we infer that the two non-magmatic sub-basins were likely established in RP3, the current phase of rifting, during which the RP1-RP2 sub-basins were largely abandoned, and strain migrated and localized both at the eastern rift margin and ahead of the initial rift termination zone.

We propose that the SRZ propagated in a pulsed manner over the three phases of extension, and we provide evidence suggesting that although the border faults largely exploited the NW-trending basement metamorphic terrane fabrics, the transient stagnation zones of the rift tips during each rift phase were influenced by rift-orthogonal terrane boundary shear zones. In essence, we argue that during the pulsed propagation of a continental rift segment, inherited strength anisotropies can serve as both strain-localizing, refracting, and possibly, temporarilyy strain-inhibiting tectonic elements in the lithosphere.

ACKNOWLEDGEMENTS

We thank Jack Williams and Ake Fagereng for their comments on the earlier versions of this manuscript which helped to improve the quality of the paper. Thanks to the Geological Survey of Malawi for providing the 2013 aeromagnetic datasets used in this study. Thanks also to the Council for Geoscience, South Africa, for providing the South African Development Community (SADC) regional aeromagnetic dataset used in this study. We thank Elias Chikalamo, Patrick R. N. Chindandali, Lois Kamuyango, Wesley T. Prater, Amy R. Pritt, Alejandra Santiago-Torres, and Kevin Vélez-Rosado for collecting field structural data in southern Malawi. We also thank Jalf Salima and Leonard Kalindekafe for supporting the logistics of our fieldwork. This research was supported by the NSF Grant No. II-1358150 and EAR 1255233.

DATA AVAILABILITY

The Shuttle Radar Topography Mission (SRTM) dataset used in this study can be freely obtained from the United States Geological Survey database https://earthexplorer.usgs.gov. The southern Malawi Total Magnetic Intensity (TMI) dataset can be freely obtained from the Interdisciplinary Earth Data Alliance (IEDA) at doi:10.1594/IEDA/324860 (Nyalugwe et al., 2019b).

REFERENCES

Addison, M.J., Rivett, M.O., Phiri, O.L., Milne, N., Milne, V., McMahon, A.D., Macpherson, L., Bagg, J., Conway, D.I., Phiri, P. and Mbalame, E., 2021. 'Hidden Hot Springs' as a Source of Groundwater Fluoride and Severe Dental Fluorosis in Malawi. Water, 13(8), p.1106.

Arkani-Hamed, J. (1988). Differential reduction-to-the-pole of regional magnetic anomalies. Geophysics, 53(12), 1592–1600.

Barr, M.W.C. and Brown, M.A., 1987. Precambrian gabbro–anorthosite complexes, Tete Province, Mozambique. Geological Journal, 22(S2), pp.139-159.

Bell, R.E., Jackson, C.A.L., Whipp, P.S. and Clements, B., 2014. Strain migration during multiphase extension: Observations from the northern North Sea. Tectonics, 33(10), pp.1936-1963.

Baranov, V. (1957). A new method for interpretation of aeromagnetic maps: Pseudo-gravimetric anomalies. Geophysics, 22(2), 359–382.

Bennett, J. D. (1989). Smaller Coal Basins in Africa Project - Final Report: Review of Lower Karoo coal basins and coal resource development in parts of central and southern Africa with particular reference to northern Malawi. British Geological Survey Technical Report WC/89/21.

Bergh, S.G., Eig, K., Kløvjan, O.S., Henningsen, T., Olesen, O. and Hansen, J.A., 2007. The Lofoten-Vesterålen continental margin: a multiphase Mesozoic-Palaeogene rifted shelf as shown by offshore-onshore brittle fault-fracture analysis. Norwegian Journal of Geology/Norsk Geologisk Forening, 87.

Bingen, B., Jacobs, J., Viola, G., Henderson, I.H.C., Skår, Ø., Boyd, R., Thomas, R.J., Solli, A., Key, R.M. and Daudi, E.X.F., 2009. Geochronology of the Precambrian crust in the Mozambique belt in NE Mozambique, and implications for Gondwana assembly. Precambrian Research, 170(3-4), pp.231-255.

Bjorlykke, K., 1989. Sedimentology and petroleum geology. Springer Berlin Heidelberg. 363p.

Bloomfield, K., 1958. The geology of the Port Herald area. Malawi Geological Survey Department Bulletin 9, Zomba.

Braun, J. (1992). Post-extensional mantle healing and episodic extension in the Canning Basin. Journal of Geophysical Research, 97(B6), 8927.

Brune, S., Heine, C., Pérez-Gussinyé, M. and Sobolev, S.V., 2014. Rift migration explains continental margin asymmetry and crustal hyper-extension. Nature communications, 5(1), pp.1-9.

Burke, K., Ashwal, L.D. and Webb, S.J., 2003. New way to map old sutures using deformed alkaline rocks and carbonatites. Geology, 31(5), pp.391-394.

Castaing, C. (1991), Post-Pan-African tectonic evolution of South Malawi in relation to the Karroo and recent East African rift systems. Tectonophysics, 191(1-2), pp.55-73.

Chisenga, C., Dulanya, Z. and Jianguo, Y. (2019), The structural re-interpretation of the Lower Shire Basin in the Southern Malawi rift using gravity data. Journal of African Earth Sciences, 149, pp.280-290.

Chorowicz, J., 2005. The east African rift system. Journal of African Earth Sciences, 43(1-3), pp.379-410.

Choubert, G., Faure-Muret, A., Chanteux, P., Roche, G., Simpson, E.S.W., Shackleton, L., Ségoufin, J., Seguin, C. and Sougy, J., 1988. International geological map of Africa. Scale 1: 5,000,000, Commission for the Geological Map of the World (CGMW), Unesco, Paris.

Cooper, W.G.G., and Bloomfield, K. 1961. The geology of the Tambani-Salambidwe area. Malawi Geological Survey Department Bulletin 13, Zomba.

Corti, G., 2004. Centrifuge modelling of the influence of crustal fabrics on the development of transfer zones: insights into the mechanics of continental rifting architecture. Tectonophysics, 384(1-4), pp.191-208.

Corti, G., 2012. Evolution and characteristics of continental rifting: Analog modeling-inspired view and comparison with examples from the East African Rift System. Tectonophysics, 522, pp.1-33.

Corti, G., van Wijk, J., Cloetingh, S. and Morley, C.K., 2007. Tectonic inheritance and continental rift architecture: Numerical and analogue models of the East African Rift system. Tectonics, 26(6).

Courtillot, V. (1982). Propagating rifts and continental breakup. Tectonics, 1(3), 239–250. https://doi.org/10.1029/TC001i003p00239

Daly, M.C., Chorowicz, J. and Fairhead, J.D., 1989. Rift basin evolution in Africa: the influence of reactivated steep basement shear zones. Geological Society, London, Special Publications, 44(1), pp.309-334.

Daly, M. C., Green, P., Watts, A. B., Davies, O., Chibesakunda, F., & Walker, R. (2020). Tectonics and Landscape of the Central African Plateau, and their implications for a propagating Southwestern Rift in Africa. Geochemistry, Geophysics, Geosystems, 21, e2019GC008746. https://doi.org/10.1029/2019G C008746

Daly, M.C., Lawrence, S.R., Kimun'a, D. and Binga, M., 1991. Late Palaeozoic deformation in central Africa: a result of distant collision?. Nature, 350(6319), pp.605-607.

Daszinnies, M.C., Emmel, B., Jacobs, J., Grantham, G.H. and Thomas, R.J., 2008. Denudation in southern Malawi and northern Mozambique: indications of the long-term tectonic segmentation of East Africa during Gonwana break-up.

Delvaux, D., 1989. The Karoo to Recent rifting in the western branch of the East-African Rift System: A bibliographical synthesis. Mus. roy. Afr. centr., Tervuren (Belg.), Dépt. Géol. Min., Rapp. ann, 1990 (1991), pp.63-83.

Delvaux, D., 2001. Karoo rifting in western Tanzania: precursor of Gondwana break-up. Contributions to geology and paleontology of Gondwana in honor of Helmut Wopfner: Cologne, Geological Institute, University of Cologne, pp.111-125.

1480 Dixey F. 1925. The Physiography of the Shire Valley, Nyasaland. Rep. Geol. Surv. Dept.,
1481 Nyasaland Proto.

1482 Donath, F.A., 1961. Experimental study of shear failure in anisotropic rocks. Geological
1483 Society of America Bulletin, 72(6), pp.985-989.

1484 Duffy, O.B., Bell, R.E., Jackson, C.A.L., Gawthorpe, R.L. and Whipp, P.S., 2015. Fault growth and
1485 interactions in a multiphase rift fault network: Horda Platform, Norwegian North Sea.
1486 Journal of Structural Geology, 80, pp.99-119.

1487 Dulanya, Z., 2017. A review of the geomorphotectonic evolution of the south Malawi rift.
1488 Journal of African Earth Sciences, 129, pp.728-738.

1489 Ebinger, C.J., Yemane, T., Harding, D.J., Tesfaye, S., Kelley, S. and Rex, D.C., 2000. Rift
1490 deflection, migration, and propagation: Linkage of the Ethiopian and Eastern rifts, Africa.
1491 Geological Society of America Bulletin, 112(2), pp.163-176.

1492 Evans, R.J., Ashwal, L.D. and Hamilton, M.A., 1999. Mafic, ultramafic, and anorthositic rocks
1493 of the Tete Complex, Mozambique: petrology, age, and significance. South African Journal of
1494 Geology, 102(2), pp.153-166.

1495 Fazlikhani, H., Aagotnes, S.S., Refvem, M.A., Hamilton-Wright, J., Bell, R., Fossen, H.,
1496 Gawthorpe, R.L., Jackson, C.A.L. and Rotevatn, A., 2020. Strain migration during multiphase
1497 extension, Stord Basin, northern North Sea rift. arthArXiv, 6 June 2020, Web:
1498 https://eartharxiv.org/b8acf/

1499 Fontijn, K., Delvaux, D., Ernst, G. G., Kervyn, M., Mbede, E., & Jacobs, P. (2010). Tectonic control
1500 over active volcanism at a range of scales: Case of the Rungwe Volcanic Province, SW
1501 Tanzania; and hazard implications. Journal of African Earth Sciences, 58(5), 764–777.

1502 Ford, M., Hemelsdaël, R., Mancini, M. and Palyvos, N., 2017. Rift migration and lateral
1503 propagation: evolution of normal faults and sediment-routing systems of the western
1504 Corinth rift (Greece). Geological Society, London, Special Publications, 439(1), pp.131-168.

1505 Fritz, H., Abdelsalam, M., Ali, K. A., Bingen, B., Collins, A. S., Fowler, A. R., et al. (2013). Orogen
1506 styles in the East African Orogen: A review of the Neoproterozoic to Cambrian tectonic
1507 evolution. Journal of African Earth Sciences, 86, 65–106.

1508 Gawthorpe, R., Leeder, M., 2000. Tectono-sedimentary evolution of active extensional basins.
1509 Basin Res. 12, 195e218.

1510 Habgood, F. (1963). The geology of the country west of the Shire River between Chikwawa
1511 and Chiromo. Malawi Geological Survey Department Bulletin No. 14, Zomba.

1512 Habgood, F., Holt, D. N., and Walshaw, R.D., 1973. The Geology of the Thyolo Area. Malawi
1513 Geological Survey Department Bulletin No. 22, Zomba.

1514 Hargrove, U.S., Hanson, R.E., Martin, M.W., Blenkinsop, T.G., Bowring, S.A., Walker, N. and
1515 Munyanyiwa, H., 2003. Tectonic evolution of the Zambezi orogenic belt: geochronological,
1516 structural, and petrological constraints from northern Zimbabwe. Precambrian Research,
1517 123(2-4), pp.159-186.

Heilman, E., Kolawole, F., Atekwana, E.A. and Mayle, M., 2019. Controls of Basement fabric on the Linkage of Rift Segments. Tectonics, 38(4), pp.1337-1366.

Henstra, G.A., Rotevatn, A., Gawthorpe, R.L. and Ravnås, R., 2015. Evolution of a major segmented normal fault during multiphase rifting: the origin of plan-view zigzag geometry. Journal of Structural Geology, 74, pp.45-63.

Heron, P.J., Peace, A.L., McCaffrey, K.J.W., Welford, J.K., Wilson, R., van Hunen, J. and Pysklywec, R.N., 2019. Segmentation of rifts through structural inheritance: Creation of the Davis Strait. Tectonics, 38(7), pp.2411-2430.

Hodge, M., Fagereng, Å., Biggs, J., & Mdala, H. (2018). Controls on early-riftgeometry: New perspectives from the Bilila-Mtakataka Fault, Malawi.Geo-physical Research Letters,45(9), 3896-3905.

Hunt, J.M., Philp, R.P. and Kvenvolden, K.A., 2002. Early developments in petroleum geochemistry. Organic geochemistry, 33(9), pp.1025-1052.

Jones-Cecil, M., 1995. Structural controls of Holocene reactivation of the Meers fault, southwestern Oklahoma, from magnetic studies. Geological Society of America Bulletin, 107(1), pp.98-112.

Katumwehe, A.B., Abdelsalam, M.G. and Atekwana, E.A., 2015. The role of pre-existing Precambrian structures in rift evolution: The Albertine and Rhino grabens, Uganda. Tectonophysics, 646, pp.117-129.

Keep, M. and McClay, K.R., 1997. Analogue modelling of multiphase rift systems. Tectonophysics, 273(3-4), pp.239-270.

Kinabo, B. D., Atekwana, E. A., Hogan, J. P., Modisi, M. P., Wheaton, D. D., & Kampunzu, A. B. (2007). Early structural development of the Okavango rift zone, NW Botswana. Journal of African Earth Sciences, 48(2-3), 125–136.

Kinabo, B.D., Atekwana, E.A., Hogan, J.P., Modisi, M.P., Wheaton, D.D. and Kampunzu, A.B., 2007. Early structural development of the Okavango rift zone, NW Botswana. Journal of African Earth Sciences, 48(2-3), pp.125-136.

Kolawole, F., Atekwana, E.A., Laó-Dávila, D.A., Abdelsalam, M.G., Chindandali, P.R., Salima, J. and Kalindekafe, L., 2018. Active deformation of Malawi rift's north basin Hinge zone modulated by reactivation of preexisting Precambrian Shear zone fabric. Tectonics, 37(3), pp.683-704.

Kolawole, F., Phillips, T.B., Atekwana, E.A. and Jackson, C.A.L., 2021a. Structural inheritance controls strain distribution during early continental rifting, rukwa rift. Frontiers in Earth Science, p.670.

Kolawole, F., Firkins, M. C., Al Wahaibi, T. S., Atekwana, E. A., & Soreghan, M. J. (2021b). Rift interaction zones and the stages of rift linkage in active segmented continental rift systems. Basin Research, 33, 2984– 3020. https://doi.org/10.1111/bre.12592

Kounoudis, R., Bastow, I.D., Ebinger, C.J., Ogden, C.S., Ayele, A., Bendick, R., Mariita, N., Kianji, G., Wigham, G., Musila, M. and Kibret, B., 2021. Body-Wave Tomographic Imaging of the

Turkana Depression: Implications for Rift Development and Plume-Lithosphere Interactions. Geochemistry, Geophysics, Geosystems, 22(8), p.e2021GC009782.

Kröner, A., Sacchi, R., Jaeckel, P., Costa, M., 1997. Kibaran magmatism and Pan-African granulite metamorphism in northern Mozambique: single zircon ages and regional implications. Journal of African Earth Sciences 25, 467–484.

Laó-Dávila, D. A., Al-Salmi, H. S., Abdelsalam, M. G., & Atekwana, E. A. (2015). Hierarchical segmentation of the Malawi Rift: The influence of inherited lithospheric heterogeneity and kinematics in the evolution of continental rifts. Tectonics, 34, 2399–2417.

Lemna, O.S., Stephenson, R. and Cornwell, D.G., 2019. The role of pre-existing Precambrian structures in the development of Rukwa Rift Basin, southwest Tanzania. Journal of African Earth Sciences, 150, pp.607-625.

Ma, G. Q., Du, X. J., Li, L. L., & Meng, L. S. (2012). Interpretation of magnetic anomalies by horizontal and vertical derivatives of the analytic signal. Applied Geophysics, 9(4), 468–474.

Mardia, K.V. and Jupp, P.E., 2009. Directional statistics. Vol. 494, John Wiley & Sons, West Sussex, England.

Manatschal, G., Lavier, L. and Chenin, P., 2015. The role of inheritance in structuring hyperextended rift systems: Some considerations based on observations and numerical modeling. Gondwana Research, 27(1), pp.140-164.

Modisi, M.P., Atekwana, E.A., Kampunzu, A.B. and Ngwisanyi, T.H., 2000. Rift kinematics during the incipient stages of continental extension: Evidence from the nascent Okavango rift basin, northwest Botswana. Geology, 28(10), pp.939-942.

Mohriak, W.U. and Leroy, S., 2013. Architecture of rifted continental margins and break-up evolution: insights from the South Atlantic, North Atlantic and Red Sea–Gulf of Aden conjugate margins. Geological Society, London, Special Publications, 369(1), pp.497-535.

Morley, C. K. (1999). Influence of preexisting fabrics on rift structure. In C. K. Morley (Ed.), Geoscience of Rift Systems—Evolution of East Africa, AAPG Studies in Geology (Vol. 44, pp. 151–160).

Morley, C. K. (2010). Stress re-orientation along zones of weak fabrics in rifts: An explanation for pure extension in 'oblique' rift segments? Earth and Planetary Science Letters, 297(3-4), 667–673.

Naliboff, J., & Buiter, S. J. H. (2015). Rift reactivation and migration during multiphase extension. Earth and Planetary Science Letters, 421, 58–67.

Nelson, R.A., Patton, T.L. and Morley, C.K., 1992. Rift-segment interaction and its relation to hydrocarbon exploration in continental rift systems (1). AAPG bulletin, 76(8), pp.1153-1169.

Njinju, E.A., Atekwana, E.A., Stamps, D.S., Abdelsalam, M.G., Atekwana, E.A., Mickus, K.L., Fishwick, S., Kolawole, F., Rajaonarison, T.A. and Nyalugwe, V.N., 2019a. Lithospheric structure of the Malawi Rift: Implications for magma-poor rifting processes. Tectonics, 38(11), pp.3835-3853.

Njinju, E.A., Kolawole, F., Atekwana, E.A., Stamps, D.S., Atekwana, E.A., Abdelsalam, M.G. and Mickus, K.L., 2019b. Terrestrial heat flow in the Malawi Rifted Zone, East Africa: Implications

for tectono-thermal inheritance in continental rift basins. Journal of Volcanology and Geothermal Research, 387, p.106656.

Nyalugwe, V.N., Abdelsalam, M.G., Atekwana, E.A., Katumwehe, A., Mickus, K.L., Salima, J., Njinju, E.A. and Emishaw, L. (2019a). Lithospheric structure beneath the Cretaceous Chilwa Alkaline Province (CAP) in southern Malawi and northeastern Mozambique. Journal of Geophysical Research: Solid Earth, 124(11), pp.12224-12240.

Nyalugwe, V.; Abdelsalam, M.; Atekwana, E.; Katumwehe, A.; Mickus, K.; Salima, J.; Njinju, E. and L. Emishaw, (2019b). 2013 Total Magnetic Intensity (TMI) gridded aeromagnetic data of southern Malawi 34 45 E – 36 00 E and 14 45 S and 16 15 S (investigator Mohamed Abdelsalam). Interdisciplinary Earth Data Alliance (IEDA). doi:10.1594/IEDA/324860.

Nyalugwe, V.N., Abdelsalam, M.G., Katumwehe, A., Mickus, K.L. and Atekwana, E.A. (2020). Structure and tectonic setting of the Chingale Igneous Ring Complex, Malawi from aeromagnetic and satellite gravity data: Implication for Precambrian terranes collision and Neogene-Quaternary rifting. Journal of African Earth Sciences, 163, p.103760.

Oesterlen, P.M. and Blenkinsop, T.G., 1994. Extension directions and strain near the failed triple junction of the Zambezi and Luangwa Rift zones, southern Africa. Journal of African Earth Sciences, 18(2), pp.175-180.

Ojo, O., Laó-Dávila, D.A. and Thomson, S.N., 2020. Thermotectonic History of the Southern Malawi Rift and Northern Shire Graben Border Faults: Insights From Apatite Fission Tracks and Remote Sensing Analyses. In AGU Fall Meeting Abstracts (Vol. 2020, pp. T024-0010).

Osagiede, E.E., Rotevatn, A., Gawthorpe, R., Kristensen, T.B., Jackson, C.A. and Marsh, N., 2020. Pre-existing intra-basement shear zones influence growth and geometry of non-colinear normal faults, western Utsira High–Heimdal Terrace, North Sea. Journal of Structural Geology, 130, p.103908.

Phillips, T.B., Fazlikhani, H., Gawthorpe, R.L., Fossen, H., Jackson, C.A.L., Bell, R.E., Faleide, J.I. and Rotevatn, A., 2019a. The Influence of Structural Inheritance and Multiphase Extension on Rift Development, the Northern North Sea. Tectonics, 38.

Phillips, T.B., Magee, C., Jackson, C.A.L. and Bell, R.E., 2018. Determining the three-dimensional geometry of a dike swarm and its impact on later rift geometry using seismic reflection data. Geology, 46(2), pp.119-122.

Phillips, T. B., and McCaffrey, K. J. W. (2019b). Terrane Boundary Reactivation, Barriers to Lateral Fault Propagation and Reactivated Fabrics: Rifting across the Median Batholith Zone, Great South Basin, New Zealand. Tectonics 38 (11), 4027–4053. doi:10.1029/2019tc005772

Phillips, T.B., Naliboff, J., McCaffrey, K., Pan, S., and van Hunen, J., 2021. The influence of crustal strength on rift geometry and development–Insights from 3D numerical modelling.

Ragland, P.C., Hatcher Jr, R.D. and Whittington, D., 1983. Juxtaposed Mesozoic diabase dike sets from the Carolinas: A preliminary assessment. Geology, 11(7), pp.394-399.

Ranalli, G. and Yin, Z.M., 1990. Critical stress difference and orientation of faults in rocks with strength anisotropies: the two-dimensional case. Journal of Structural geology, 12(8), pp.1067-1071.

1637 Ring, U., 1995. Tectonic and lithological constraints on the evolution of the Karoo graben of
1638 northern Malawi (East Africa). Geologische Rundschau, 84(3), pp.607-625.

1639 Rotevatn, A., Kristensen, T., Ksienzyk, A., Wemmer, K., Henstra, G., Midtkandal, I., Grundvåg,
1640 S.A., Andresen, A., 2018. Structural inheritance and rapid rift-length establishment in a
1641 multiphase rift: the East Greenland rift system and its Caledonian orogenic ancestry.
1642 Tectonics 37, 1858–1875.

1643 Ryan, W. B. F., S.M. Carbotte, J. Coplan, S. O'Hara, A. Melkonian, R. Arko, R.A. Weissel, V.
1644 Ferrini, A. Goodwillie, F. Nitsche, J. Bonczkowski, and R. Zemsky (2009), Global Multi-
1645 Resolution Topography (GMRT) synthesis data set, Geochem. Geophys. Geosyst., 10, Q03014.

1646 Sacchi, R., Cadoppi, P. and Costa, M., 2000. Pan-African reactivation of the Lurio segment of
1647 the Kibaran Belt system: a reappraisal from recent age determinations in northern
1648 Mozambique. Journal of African Earth Sciences, 30(3), pp.629-639.

1649 Scholz, C.A., Shillington, D.J., Wright, L.J., Accardo, N., Gaherty, J.B. and Chindandali, P., 2020.
1650 Intrarift fault fabric, segmentation, and basin evolution of the Lake Malawi (Nyasa) Rift, East
1651 Africa. Geosphere.

1652 Singh, A.K., Singh, M.P., Sharma, M. and Srivastava, S.K., 2007. Microstructures and
1653 microtextures of natural cokes: a case study of heat-affected coking coals from the Jharia
1654 coalfield, India. International Journal of Coal Geology, 71(2-3), pp.153-175.

1655 Smets, B., Delvaux, D., Ross, K.A., Poppe, S., Kervyn, M., d'Oreye, N. and Kervyn, F. (2016). The
1656 role of inherited crustal structures and magmatism in the development of rift segments:
1657 Insights from the Kivu basin, western branch of the East African Rift. Tectonophysics, 683,
1658 pp.62-76.

1659 Stamps, D.S., Saria, E. and Kreemer, C. (2018). A geodetic strain rate model for the East
1660 African Rift system. Scientific reports, 8(1), pp.1-8.

1661 Stevens, V.L., Sloan, R.A., Chindandali, P.R., Wedmore, L.N., Salomon, G.W. and Muir, R.A.,
1662 2021. The Entire Crust can be Seismogenic: Evidence from Southern Malawi. Tectonics,
1663 p.e2020TC006654.

1664 Stewart, A.K., Massey, M., Padgett, P.L., Rimmer, S.M. and Hower, J.C., 2005. Influence of a
1665 basic intrusion on the vitrinite reflectance and chemistry of the Springfield (No. 5) coal,
1666 Harrisburg, Illinois. International Journal of Coal Geology, 63(1-2), pp.58-67.

1667 Suárez-Ruiz, I. and Crelling, J.C. eds., 2008. Applied coal petrology: the role of petrology in
1668 coal utilization. 1st edition, Academic press, Elsevier Ltd, New York. 408p.
1669 https://doi.org/10.1016/B978-0-08-045051-3.X0001-2

1670 Trouw, R.A. and De Wit, M.J., 1999. Relation between the Gondwanide Orogen and
1671 contemporaneous intracratonic deformation. Journal of African Earth Sciences, 28(1),
1672 pp.203-213.

1673 Versfelt, J.W. (2009), South Atlantic margin rift basin asymmetry and implications for pre-
1674 salt exploration. International Petroleum Technology Conference (IPTC) paper 13833, Doha,
1675 Qatar.

Wheeler, W. H., & Karson, J. A. (1989). Structure and kinematics of the Livingstone Mountains border fault zone, Nyasa (Malawi) Rift, southwestern Tanzania. Journal of African Earth Sciences (and the Middle East), 8(2–4), 393–413.

Wheeler, W.H. and Karson, J.A., 1994. Extension and subsidence adjacent to a "weak" continental transform: An example from the Rukwa rift, East Africa. Geology, 22(7), pp.625-628.

Williams, J.N., Fagereng, Å., Wedmore, L.N., Biggs, J., Mphepo, F., Dulanya, Z., Mdala, H. and Blenkinsop, T., 2019. How do variably striking faults reactivate during rifting? Insights from southern Malawi. Geochemistry, Geophysics, Geosystems, 20(7), pp.3588-3607.

Williams, J.N., Mdala, H., Fagereng, Å., Wedmore, L.N., Biggs, J., Dulanya, Z., Chindandali, P. and Mphepo, F., 2021. A systems-based approach to parameterise seismic hazard in regions with little historical or instrumental seismicity: active fault and seismogenic source databases for southern Malawi. Solid Earth, 12(1), pp.187-217.

Wedmore, L.N., Williams, J.N., Biggs, J., Fagereng, Å., Mphepo, F., Dulanya, Z., Willoughby, J., Mdala, H. and Adams, B., 2020a. Structural inheritance and border fault reactivation during active early-stage rifting along the Thyolo fault, Malawi. Journal of Structural Geology, p.104097.

Wedmore, L.N., Biggs, J., Williams, J.N., Fagereng, Å., Dulanya, Z., Mphepo, F. and Mdala, H., 2020b. Active fault scarps in southern Malawi and their implications for the distribution of strain in incipient continental rifts. Tectonics, 39(3), p.e2019TC005834.

Wedmore, L.N., Biggs, J., Floyd, M., Fagereng, Å., Mdala, H., Chindandali, P., Williams, J.N. and Mphepo, F., 2021. Geodetic constraints on cratonic microplates and broad strain during rifting of thick Southern African lithosphere. Geophysical Research Letters, 48(17), p.e2021GL093785.

Westerhof, A.P., Lehtonen, M.I., Mäkitie, H., Manninen, T., Pekkala, Y., Gustafsson, B. and Tahon, A., 2008. The Tete-Chipata Belt: A new multiple terrane element from western Mozambique and southern Zambia. Geological Survey of Finland Special Paper, 48, pp.145-166.

Woolley, A. R., Bevan, J. C. and Elliott, C. J. (1979). The Karroo dolerites of southern Malawi and their regional geochemical implications. Mineralogical Magazine, 43(328), p.487-495.

Youash, Y., 1969. Tension tests on layered rocks. Geological Society of America Bulletin, 80(2), pp.303-306.